Research Paper

GEOSPHERE

GEOSPHERE, v. 20, no. 1

https://doi.org/10.1130/GES02651.1

8 figures; 3 tables; 1 set of supplemental files

CORRESPONDENCE: rgallo@hawaii.edu

CITATION: Gallo, R.I., Ort, M.H., Iacovino, K., Silleni, A., Smith, V.C., Giordano, G., Isaia, R., and Boro, J., 2024, Reconciling complex stratigraphic frameworks reveals temporally and geographically variable depositional patterns of the Campanian Ignimbrite: Geosphere, v. 20, no. 1, p. 1–22, https://doi.org/10.1130/GES02651.1.

Science Editor: David E. Fastovsky
Associate Editor: Jan Marie Lindsay

Received 16 February 2023
Revision received 8 September 2023
Accepted 27 September 2023

Published online 13 December 2023

Reconciling complex stratigraphic frameworks reveals temporally and geographically variable depositional patterns of the Campanian Ignimbrite

Rose I. Gallo[1,2], Michael H. Ort[2], Kayla Iacovino[3], Aurora Silleni[2,5], Victoria C. Smith[4], Guido Giordano[5], Roberto Isaia[6], and Joseph Boro[7]

[1]Department of Earth Sciences, University of Hawai'i at Mānoa, 1680 East-West Road, Honolulu, Hawaii 96822, USA
[2]School of Earth and Sustainability, Northern Arizona University, Flagstaff, Arizona 86011, USA
[3]Jacobs, NASA Johnson Space Center, Houston, Texas 77058, USA
[4]Research Laboratory for Archaeology and the History of Art, School of Archaeology, University of Oxford, 1 South Parks Road, Oxford OX1 3TG, UK
[5]Dipartimento di Scienze, Sezione Geologia, Università Roma Tre, Largo San Leonardo Murialdo 1, 00146 Roma, Italy
[6]Istituto Nazionale di Geofisica e Vulcanologia, Osservatorio Vesuviano, 80124 Naples, Italy
[7]Lawrence Livermore National Laboratory, Livermore, California 94550, USA

ABSTRACT

The 39.8-ka Campanian Ignimbrite was emplaced during a large caldera-forming eruption of Campi Flegrei near Naples, Italy. The ignimbrite is found up to 80 km from the caldera, and co-ignimbrite ash-fall deposits occur 3200 km away. The proximal and distal stratigraphy of the Campanian Ignimbrite has not been definitively correlated due to the dissimilar appearance of the proximal and distal deposits, a lack of medial exposures, and the inconsistency and heterogeneity of the proximal stratigraphy. Here, we document the major-element glass-shard chemistry, matrix componentry, and lithic componentry of the proximal and distal stratigraphic sequences of the ignimbrite to attempt to correlate the units. The results of these disparate observations taken together suggest that the established stratigraphic units cannot be directly and uniquely correlated between the proximal and distal regions and that neither the proximal nor distal stratigraphy provides a record of the entire eruptive sequence. However, the characteristics studied can be used to demarcate eruptive phases that are connected to some of the defined units in the proximal and distal stratigraphy.

1. INTRODUCTION

The 39.8-ka Campanian Ignimbrite is associated with the first caldera-forming eruption of Campi Flegrei caldera, which is near Naples, Italy (Fig. 1; Fedele et al., 2008). This eruption was the largest volcanic event in Europe in the last 200 k.y. (De Vivo et al., 2001), emplacing 181–265 km^3 dense rock equivalent (DRE) of pyroclastic material (Fig. 1; Rosi et al., 1999; Silleni et al., 2020). The eruption started with the generation of a Plinian column that dispersed ash and lapilli to the east and south (Rosi et al., 1999; Cappelletti et al., 2003), followed by pyroclastic density currents (PDCs), which deposited the Campanian Ignimbrite and generated co-ignimbrite plumes that dispersed ash 3200 km away across eastern Europe and western Asia (Perrotta and Scarpati, 2003; Pyle et al., 2006; Anikovich et al., 2007; Costa et al., 2012; Smith et al., 2016).

One of the major barriers to developing a complete reconstruction of the Campanian Ignimbrite eruption is the lack of coherent stratigraphy to correlate the proximal and distal ignimbrite deposits. The Campanian Ignimbrite shows a great disparity in appearance between the proximal and distal ignimbrite, and some early workers doubted whether they originated from the same eruption (Di Girolamo et al., 1984; Lirer et al., 1991). The Tyrrhenian Sea lies to the west of the caldera, so about half of the PDC runout area is over sea where any resulting deposits are inaccessible. The proximal terrestrial deposits, those within roughly 8 km of the caldera rim, are very coarse grained, and include breccias; fiamme- or lithic-rich, high-grade ignimbrite; and beds of spatter bombs. In this proximal setting, there is substantial heterogeneity in the stratigraphy and deposit characteristics of the exposures. The distal deposits, ~25–80 km from the caldera, consist of lithic- and pumice-bearing, incipiently welded-to-nonwelded, lithified-to-unconsolidated ignimbrite dominated by a fine-ash matrix. The lateral continuity of the proximal and distal deposits is obscured by an absence of medial (~8–25 km from vent) exposures due to burial beneath volcanic and sedimentary deposits on the Campanian plain (Orsi et al., 1996; Silleni et al., 2020).

Descriptions of medial deposits are limited to samples collected in boreholes, including those discussed in Isaia et al. (2018). The correlation of the

Rose Gallo https://orcid.org/0000-0002-2576-4221

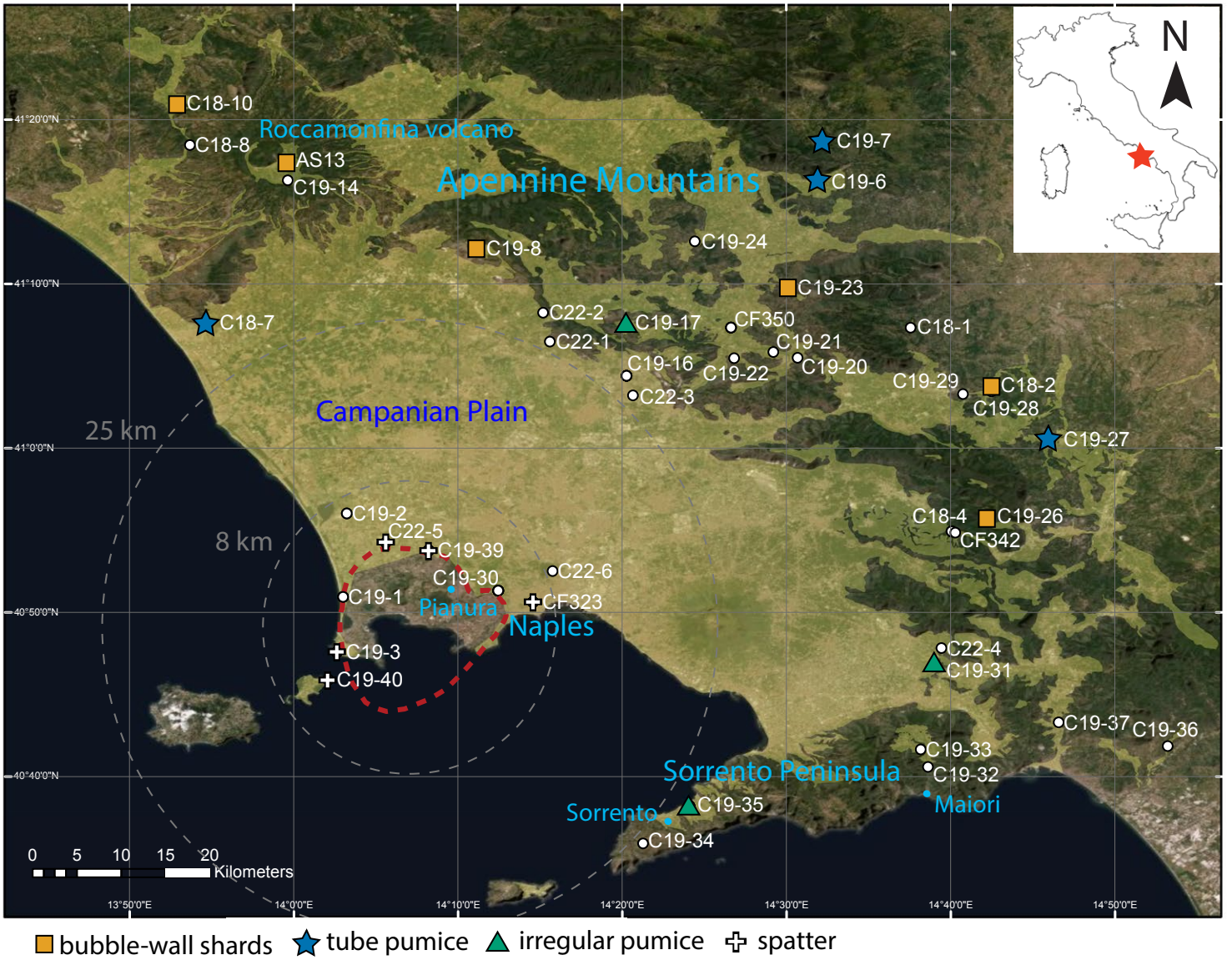

Figure 1. Map showing locations of all sample sites used in this study (location codes are given in Table 2), the hypothesized overall distribution of the Campanian Ignimbrite (in yellow; Silleni et al., 2020), and the approximate outline of Campi Flegrei caldera (red dashed line; based on Vitale and Isaia, 2014). Inset shows the location of Campi Flegrei in Italy. Orange squares, blue stars, and green triangles indicate the dominant matrix-type in Welded Grey Ignimbrite (WGI) exposures, and white points are used for all other exposures. Dashed circles show the approximate boundaries between the proximal, medial, and distal deposits of the ignimbrite. Map was created with ArcGIS and Adobe Illustrator.

deposits was based on mapping (Rosi et al., 1996; Scarpati et al., 2020), remanent magnetization (Ort et al., 1999), dating (DeVivo et al., 2001; Fedele et al., 2008; Giaccio et al., 2008, 2017; Douka et al., 2010), and glass geochemistry (Fedele et al., 2008, 2016; Forni et al., 2016; Smith et al., 2016; Di Salvo et al., 2020). Separate schemes for the proximal and distal stratigraphy were developed by several authors (Table 1).

1.1 Distal Stratigraphy

The distal deposits of the Campanian Ignimbrite are ash-rich ignimbrite. The ignimbrite has a low aspect ratio (the ratio of ignimbrite thickness to lateral extent; $9.84*10^{-5}$; Silleni et al., 2020), which is often used as an indicator of PDC energy (Giordano and Cas, 2021). It exhibits massive valley-pond facies, and thin outcrops occur at high elevations, but these lack the crossbedding or sorting of a classic veneer facies (a thin, topography-mantling ignimbrite deposit observed on slopes and areas of higher elevation; Wilson and Walker, 1982; Rosi et al., 1996; Perrotta et al., 2010; Scarpati et al., 2015a; Fedele et al., 2016; Silleni et al., 2020; Giordano and Cas, 2021). The distal deposits have been divided into four units, from bottom to top (Cappelletti et al., 2003; Sparice, 2015; Fedele et al., 2016). The ignimbrite sits atop the Plinian Pumice Fall (PPF) that is present to the south and east of the caldera. These are the Unconsolidated Stratified Ash Flow (USAF), the Welded Grey Ignimbrite (WGI), the Lithified Yellow Tuff (LYT), and the Coarse Pumice Flow (CPF) (Table 1; Fig. 2). The USAF consists of unconsolidated, stratified ash and lapilli with discontinuous lithic- and crystal-rich horizons near the base. This unit has been interpreted as a depositional facies akin to a ground layer or a discontinuous version of Wilson and Walker's (1982) Layer 1H for this ignimbrite (Scarpati et al., 2015b). The WGI, contrary to its name, is only incipiently welded to unconsolidated (Fedele et al., 2016). The LYT is typically distinguished by extensive post-emplacement zeolitization that imparts a yellow color to the deposit (Fedele et al., 2008). The WGI and LYT are commonly interpreted as being distinguished only by their alteration facies (Cappelletti et al., 2003; Langella et al., 2013; Fedele et al., 2016). The WGI is more broadly distributed and is typically thicker than the LYT (Sparice, 2015; Fedele et al., 2016). The uppermost layer, the CPF, has only been described in four exposures and is found above the LYT or the WGI at different outcrops and is described as an unconsolidated, pumice lapilli- and block-rich unit with a reversely graded pumice concentration zone at its top (Cappelletti et al., 2003; Scarpati et al., 2015b; Fedele et al., 2016).

1.2 Proximal Stratigraphy

The proximal deposits of the Campanian Ignimbrite eruption are thin and patchy considering the thickness of the distal deposits. Proximal deposits just outside the caldera reach a maximum of 80 m thick, but outcrops of the distal deposits 45 km from the caldera center at the foot of the Apennine Mountains are 30 m thick, and some outcrops 60 km away are 20 m thick (Silleni et al., 2020). The entire Campanian Ignimbrite thickness inside the caldera, based upon drill cores, is less than 250 m (De Natale et al., 2016). The proximal exposures are not laterally continuous and are typically found on the sides of paleohills, mostly on slopes facing the caldera. Even in thick sequences where the stratigraphy appears relatively complete, substantial differences between outcrops are evident in terms of the presence, thickness, and even the order of some of the proposed units. Additionally, there is substantial heterogeneity in deposit characteristics within units. This complexity has resulted in two different naming conventions for the proximal deposits and their units, one by Rosi et al. (1996) and another proposed originally by Perrotta and Scarpati (1994) and modified into the current scheme by Fedele et al. (2008; Table 1). The two schemes overlap considerably, but none of the units defined in each correlates directly to one another.

TABLE 1. CLASSIFICATION SCHEMES FOR PROXIMAL UNITS AND DISTAL UNITS

<table>
<tr><th colspan="4">Proximal</th><th>Distal</th></tr>
<tr><th colspan="2">Perrotta and Scarpati (1994)</th><th>Melluso et al. (1995)</th><th>Rosi et al. (1996)</th><th colspan="2">Fedele et al. (2008)</th><th>Cappelletti et al. (2003)</th></tr>
<tr><td rowspan="3">Breccia Museo Member</td><td>UPFU</td><td>UPFU</td><td>D</td><td rowspan="5">Breccia Museo Formation</td><td>UPFU</td><td>CPF</td></tr>
<tr><td>BU/SU</td><td>BU/SU</td><td>C</td><td>BU/SU</td><td>LYT</td></tr>
<tr><td>LPFU</td><td>LPFU</td><td>B</td><td>LPFU</td><td rowspan="2">WGI</td></tr>
<tr><td rowspan="2"></td><td>Piperno</td><td rowspan="2"></td><td rowspan="2">A</td><td>Piperno</td></tr>
<tr><td>USAF</td><td>USAF</td><td>USAF</td></tr>
<tr><td colspan="2">PPF</td><td>PPF</td><td>PPF</td><td colspan="2">PPF</td><td>PPF</td></tr>
</table>

Notes: Perrotta and Scarpati (1994) did not attribute the proximal stratigraphy to the Campanian Ignimbrite eruption. Classification schemes for the proximal and distal units are from the literature. BU—Breccia Unit, CPF—Coarse Pumice Flow, LPFU—Lower Pumice Flow Unit, LYT—Lithified Yellow Tuff, PPF—Plinian Pumice Fall, SU—Spatter Unit, UPFU—Upper Pumice Flow Unit, USAF—Unconsolidated Stratified Ash Flow, WGI—Welded Grey Ignimbrite.

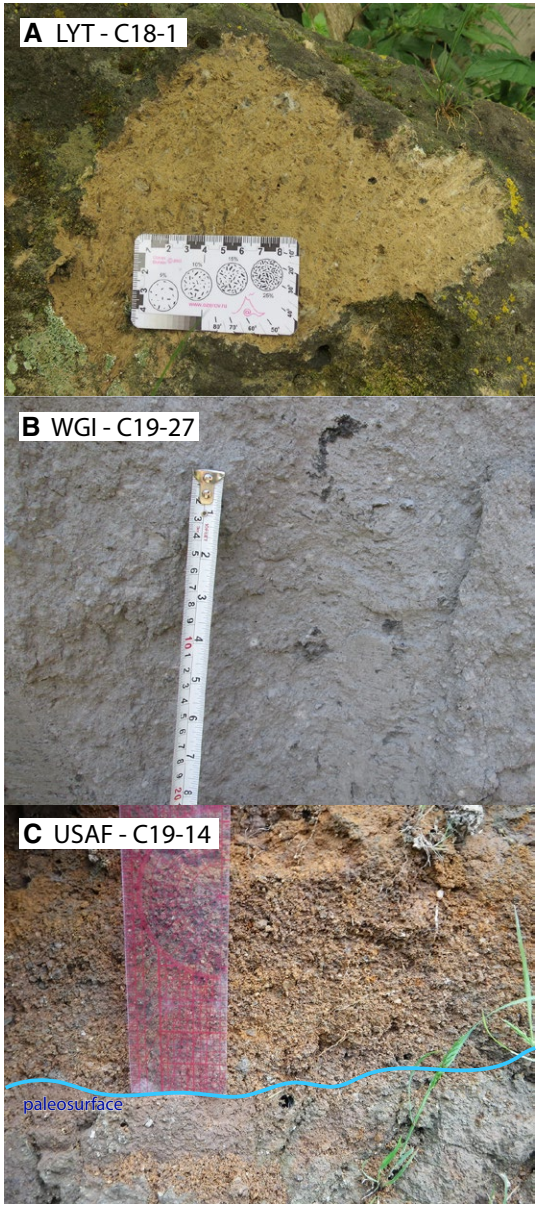

Figure 2. Examples of the distal units, from top to bottom, following the classification scheme of Fedele et al. (2008). (A) Lithified Yellow Tuff (LYT), (B) Welded Grey Ignimbrite (WGI), and (C) Unconsolidated Stratified Ash Flow (USAF). Location codes correspond to points in Figure 1.

The naming convention presented by Perrotta and Scarpati (1994) and Fedele et al. (2008) for the proximal stratigraphy defines six units in the ignimbrite sequence, labeled the Breccia Museo Formation by Fedele et al. (2008). These are the Unconsolidated Stratified Ash Flow (USAF), Piperno, Lower Pumice Flow Unit (LPFU), Breccia Unit (BU), Spatter Unit (SU), and Upper Pumice Flow Unit (UPFU)(Table 1; Fig. 3). The designation of a basal USAF in both the proximal and distal deposits is based upon similarities of the appearance of the deposits. The Piperno unit is stratigraphically above the USAF unit; contains the most densely welded sections of ignimbrite; and includes beds of coarse, matrix-supported breccia and fiamme-rich ignimbrite. Some exposures contain both clast types in alternating horizons, and some contain only breccias of variable welding and matrix content (Fedele et al., 2016). The LPFU is typically identified by the presence of pumice- or ash-rich deposits of variable sorting, grading, and consolidation. The BU is a coarse, clast-supported, lithic-rich breccia containing lesser amounts of pumice, scoria, and obsidian. The BU contains a diversity of lithic types at different exposures, including lavas, pyroclastic rocks, sedimentary rocks, plutonic rocks, fumarole deposits, and rocks that were hydrothermally altered to various extents (Rosi et al., 1996). This unit is bedded or graded in places and is interspersed in its lower portions with the SU, which consists of spatter-rich horizons with minor welded ash and lithic lapilli (Fedele et al., 2008). The uppermost unit is the UPFU, which consists of poorly sorted, variably consolidated, pumice-dominated beds that are massive or slightly normally graded. Some exposures contain spatter clasts. In some exposures to the north and east of the caldera, the pumice and matrix material is rich in coarse sanidine crystals. Not all exposures have all of the units, and the USAF, Piperno, and LPFU may each be absent from the sequence in some locations, in which case the BU or SU sits directly on the PPF or the paleosurface (Fedele et al., 2016).

In a comprehensive study of all proximal stratigraphic sections known at that time, Rosi et al. (1996) defined four units for the proximal ignimbrite deposits, A–D from bottom to top, although they never observed all four units at one exposure. Unit A, identified at only one location near C19-30 (Fig. 1), is composed of layers of gray eutaxitic tuff with numerous fiamme and few lithic clasts alternating with lithic breccias with clasts consisting of primarily gray trachytes. Unit B is composed of a combination of sintered ignimbrite, low-grade ignimbrite, and lithic-rich breccias. In Rosi et al.'s (1996) stratigraphic columns, Unit C typically consists of a lithic breccia many meters or tens of meters thick that contains a horizon of spatter agglutinate typically within its lower third. Unit D is a low-grade ignimbrite with large pumice clasts at the top of the sequence. Rosi et al.'s (1996) Unit A corresponds to a single exposure defined as Piperno in Fedele et al. (2016). Unit B corresponds to all materials classified as LPFU and proximal USAF using the Fedele et al. (2008) scheme, as well as some portions of selected exposures that were classified as Piperno and BU. Unit C is entirely BU and SU, except for the lower beds at Punta Marmolite (C19-39C to C19-39F). Unit D corresponds to the UPFU of Fedele et al. (2008). The relations between the two schemes at all outcrops sampled for this work can be seen in Figure 5A.

Figure 3. Examples of each of the main proximal ignimbrite units, the Piperno, Lower Pumice Flow Unit (LPFU), Breccia Unit (BU), and Upper Pumice Flow Unit (UPFU) in Fedele et al.'s (2008) scheme, from bottom (left column) to top (right column). Each image is labeled with the sample code taken at that location and the Rosi et al. (1996) unit designation, if it has one. Two images are from exposures that were not sampled for this study: Pianura is marked on Figure 1, and Vigna San Martino is near outcrop CF323.

1.3 Correlation Efforts

Perrotta et al. (2006) inferred that the Piperno, which is observed in the proximal stratigraphy, and the WGI, which dominates the distal stratigraphy, could be correlative units based on observations of a single exposure, described as transitional in appearance between the two, to the west of Vomero Hill (close to CF323) in Naples. No detailed stratigraphic section or photograph of this exposure was published. Based on this correlation, Fedele et al. (2016) suggested that the LPFU, BU/SU, and UPFU are exclusively proximal units with no distal correlative units. They accepted the hypothesis of Cappelletti et al. (2003) that the LYT is an alteration facies of the WGI and therefore correlated all distal deposits to the Piperno. Observations of drill cores in the northern Campanian plain by Isaia et al. (2018) and Ruberti et al. (2020) identified Piperno-like materials within the lower portions of the WGI at some locations. These tentatively proposed correlations are based on limited observations of a highly heterogeneous set of deposits with inconsistently defined unit schemes, and the exact relation between the visually distinguishable portions of the proximal and distal deposits is far from established.

In this study, we compare observations of glass compositions, glass shard shapes, and lithic componentry among the proximal and distal deposits with reference to the units defined by the stratigraphic schemes of both Fedele et al. (2008) and Rosi et al. (1996). Our purpose is to determine if it is possible to correlate the proximal and distal deposits of the Campanian Ignimbrite using these characteristics and whether the correlations coincide with the existing stratigraphic schema. The PPF is not a focus of this study, as it has been well mapped and chemically characterized (Rosi et al., 1999; Polacci et al., 2003; Scarpati and Perrotta, 2016). We utilize the published schema of Rosi et al. (1996) and Fedele et al. (2008) in our attempts to correlate the units, rather than create yet another set of stratigraphic nomenclature. However, we aim to observe trends in the deposits outside of the existing stratigraphic frameworks before applying the unit schemes and evaluating their utility in representing the stratigraphy with regards to changes in magmatic sources, eruptive processes, vent locations, and dynamics throughout the eruption. We use this information to add to the interpretation of the eruptive sequence. We propose that the Campanian Ignimbrite was produced by an eruption that left a heterogeneous and incomplete depositional record at all localities.

2. METHODS

Bulk samples of Campanian Ignimbrite material were collected from previously identified stratigraphic units at 43 localities; multiple samples were taken in vertical sections at 16 of these (Fig. 1). Sites were selected from known exposure locations to provide samples from a variety of defined units, at various heights above the basal contact within the stratigraphy, from high and low elevations, and from various azimuths from the caldera. All previously described proximal units from the scheme of Rosi et al. (1996), and all units from the scheme of Fedele et al. (2008) except for the proximal USAF, were sampled. Observations of two outcrops identified in Fedele et al. (2016) as containing exposures of the CPF, C22-2, and CF351, did not reveal any deposit distinguishable as a separate unit from the WGI and LYT observed in those locations, respectively. The size and abundance of pumice clasts increases near the top of these outcrops, but the difference is gradual and subtle. We therefore note that the samples taken in the zone of pumice concentration at these two outcrops, C22-2 and CF352, are probably equivalent to what Fedele et al. (2016) labeled as CPF, but if not, we did not sample this unit. The unit designations for each of the exposures were taken from Rosi et al. (1996), Fedele et al. (2008), or Sparice (2015) and are indicated in File S2 in the Supplemental Material.[1] Lithic clasts from samples at each of 23 exposures were identified based on their hand-sample characteristics. All lithic clasts greater than 1 mm in size were classified in most samples, except in samples where many hundreds of lithic clasts were present and a random sample of >50 clasts was selected. The presence or absence of obsidian clasts was also noted for each sample. The matrix componentry, including the variety of glass shard types within the 2–3.5 Φ size range, was determined for all samples by visual estimation and for 29 samples by point counting at least 200 grains using a picking microscope. A magnet was passed over a portion of the materials for each sample to observe the presence or absence of magnetite; no adequate interpretation of the pattern of these data could be made, but it is included in File S3 (see footnote 1).

Grain mounts of matrix ash were used for both electron microprobe (EPMA) analysis of major-element geochemistry and secondary electron imaging of glass shards using a ZEISS Supra 40VP field emission–scanning electron microscope. Fragments of pumice lapilli, spatter, and fiamme were also analyzed for major-element composition by EPMA at the University of Hawai'i at Mānoa, Oxford University, and NASA Johnson Space Center. Counts were obtained for the standard set of major elements and Cl. The analysis was run at 15 kV and 5–6 nA using a beam diameter of 10 µm or 3 µm, depending on the available flat surface size of clean glass. Secondary electron images of each type of matrix glass shard from the same grain mounts, as well as two grain mounts containing ignimbrite and ultra-distal co-ignimbrite shards of mixed sizes, were obtained using an accelerating voltage of 10 keV, a scanning speed of 1.5 min, and a magnification of 30× for the ignimbrite samples and 70× for the co-ignimbrite samples with a standard aperture size. Further details on sample preparation and analytical methods can be found in the Supplemental Material.

[1]Supplemental Material. File S1 includes an elaboration of our methods, a figure portraying our geochemical data in greater detail, and a figure showing some trends in quantitative shard shape parameters. File S2 is a catalog of all the samples used in our study with an image of the exposure. File S3 is a series of Excel documents containing all data sets. Please visit https://doi.org/10.1130/GEOS.S.24286873 to access the supplemental material, and contact editing@geosociety.org with any questions.

3. RESULTS

3.1 Matrix Componentry

Seven types of juvenile glass shards were identified in scanning electron microscope images of the matrix ash of the Campanian Ignimbrite: scoria, elongate pumice, tube pumice, irregular dense pumice, irregular less-dense pumice, bubble-wall shards, and blocky shards (Fig. 4). Scoria are distinguished by their large bubbles and thick glass septa relative to particle size (scoria is used here purely as a textural term; the different shard types show no relation to chemical composition). Elongate pumice clasts generally have elongated particle shapes and vesicles but differ from the tube pumice in that they lack symmetrical stick-like shapes, and the vesicles do not extend the length of the particle perfectly parallel to the long axis. The two types of irregular pumice both have rounded or lumpy irregular shapes, with no elongation and small vesicles, but are distinguished by their vesicularity. The dense irregular pumice has fewer vesicles, or its vesicles may be filled in by weathering or alteration products. Clasts classified as dense irregular pumice were, in some cases, difficult to distinguish from clusters of finer ash that were not fully disaggregated. However, this shard type is found in a minority of samples and is not useful for classification, so this source of error in our classification scheme is not important. Bubble-wall shards have arcuate shapes or form complete circles around vesicles that are much larger than those observed in the pumice clasts; a single vesicle or the partial outline of a single vesicle up to ~1 mm in size dominates the shape of the bubble-wall shards. Blocky shards have angular, polygonal shapes and have few or no vesicles inside. Quantitative analysis of the shard shapes was undertaken using PARTISAN (Dürig et al., 2018) to determine if shard types could be distinguished using empirical shape parameters. Methods and results of this analysis are provided in File S1.

Componentry of the ignimbrite matrix material at the 2–3.5 Φ size reveals three general types of matrix. This characterization was made with a reflected light microscope, with which only five shard types could be distinguished; the elongate and tube-pumice shards cannot be differentiated under lower magnification, nor can the two types of irregular pumice, so we combine these pairs into tube and irregular pumice shard types, respectively. The most common matrix type, which we refer to as tube-pumice–dominated, consists primarily of tube/elongate pumice shards with lesser amounts of bubble-wall shards, free crystals, lithic clasts, and—in some samples—small amounts of scoria, obsidian, or blocky shards. The shapes of the shards are consistent in all samples with this matrix type, but other features, such as color, vary among samples. The second matrix type, referred to as irregular-pumice–dominated, consists primarily of irregular rounded pumice shards with small quantities of crystals and lithic clasts and minor amounts of tube pumice, bubble-wall shards, obsidian, scoria, blocky shards, and fragments of fiamme in some samples. The third matrix type, which we refer to as bubble-wall-shard dominated, consists primarily of gray bubble-wall shards

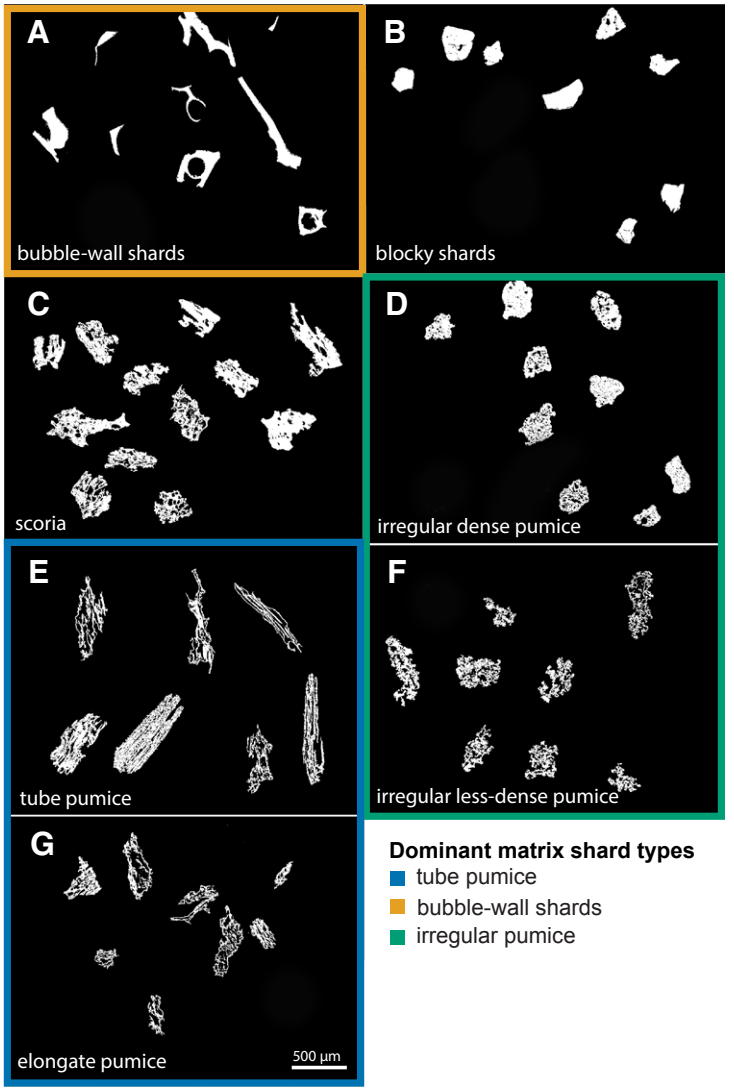

Figure 4. Examples of the seven shard types identified in the Campanian Ignimbrite deposits: (A) bubble-wall shards, (B) blocky shards, (C) scoria, (D) irregular dense pumice, (E) tube pumice, (F) irregular less-dense pumice, and (G) elongate pumice, shown in binary images created from secondary electron images. The three dominant ash shard types distinguishable at low magnification are demarcated into groups by color. Scale is the same for all images.

with subordinate tube-pumice shards, crystals, lithic clasts, and scarce scoria. All samples, therefore, contain more than one shard type, but most show a prevalence of one type over the others. Figure 5B shows the three matrix types found within the samples.

Tube-pumice–dominated matrix is found in just under half the distal samples analyzed and half of the proximal samples. It is found throughout the stratigraphy of the distal deposits and generally in the middle of the stratigraphy of the proximal deposits. Irregular-pumice–dominated matrix is observed in one-sixth of distal samples analyzed and half of the proximal samples analyzed. It is observed near the base of the distal deposits and near the top and bottom of the proximal deposits. The bubble-wall-shard dominated matrix is found only in the distal exposures, in one-third of the samples analyzed. Co-ignimbrite samples from the seafloor of the Mediterranean Sea and the Ionian Sea (see Table 2 for coordinates of the cores) contain an even higher proportion of bubble-wall shards than the ignimbrite samples.

Considering the existing stratigraphic schemes, tube-pumice–dominated matrix was observed in all samples of the proximal BU and the distal LYT, about one-third of samples of the distal WGI, and one LPFU sample within the framework of Fedele et al. (2008; Figs. 5A and 5B). It is therefore found in all Unit C samples and some Unit B samples within the framework of Rosi et al. (1996). In the LYT, matrix shards are altered to zeolites and clays and are no longer glassy, but they retain their original shapes. Irregular-pumice–dominated matrix is found in the proximal Piperno, UPFU, one sample of the LPFU, one sample that is deemed ambiguous Piperno and/or BU (C19-2b), and three samples of the WGI. This means that samples of Units A and D, and some of Unit B, have this matrix style. Bubble-wall-shard dominated matrix is found exclusively in the WGI. The LPFU in Fedele et al.'s (2008) proximal scheme, Unit B in Rosi et al.'s (1996) proximal scheme, and the distal WGI each contain more than one matrix type across different outcrops; therefore, the defined units cannot be uniquely identified by matrix type.

The geographic distribution of matrix styles among outcrops assigned to the WGI reveals a few potential patterns (Fig. 1; Table 2). Within the WGI, which accounts for most of the volume of the distal deposits, exposures containing irregular-pumice–dominated matrix tend to be 45 km or less from the approximate center of the caldera and are not separated from the caldera by any high ridges. For two of the sites (C19-31 and C19-35; Fig. 1), a direct flow path from the caldera crosses the Bay of Naples. The bubble-wall-shard dominated samples include samples taken from sites on and behind ridges in the Apennines. Two samples, C19-26a and AS13, have a significantly higher percentage of bubble-wall shards than other samples, although they are still less abundant than in the ultra-distal co-ignimbrite samples. They were collected from high-elevation outcrops, at 970 m asl on the up-current slope of a 1400-m-high ridge in the Apennines and inside of Roccamonfina caldera at 445 m asl, respectively. Tube-pumice–dominated samples are found in the three most distal ignimbrite exposures, which are behind several ridges, but also one exposure on the Campanian plain at the foot of a ridge 39.5 km from the caldera center (Fig. 1).

3.2 Major-Element Glass Chemistry

Major-element glass composition from matrix shards, pumice lapilli, fiamme, and spatter were examined and compared to data from the literature for pumice lapilli glass (Melluso et al., 1995; Civetta et al., 1997; Signorelli et al., 1999; Fulignati et al., 2004; Fedele et al., 2008, 2016; Forni et al., 2016; Smith et al., 2016; Di Salvo, 2018) to identify any trends within or between the proximal and distal deposits and to facilitate correlation. No relation between the shard shapes and chemistry of glass shards was found. All data are described and provided in the Supplemental Material. With the combination of new data and previously reported data from the literature, four compositional clusters, best observed in plots of SiO_2, MgO, CaO, Na_2O, and K_2O, can be distinguished (Fig. 6). Clusters 1 and 2 represent most of the data, with clusters 3 and 4 each found at a single exposure. Cluster 1 shows very little variation in MgO, CaO, Na_2O, and K_2O with SiO_2. It occupies a range of roughly 60–64 wt% SiO_2, 2.6–3.5 wt% FeO, 0.2–0.4 wt% MgO, 1.5–2.0 wt% CaO, 5.5–7.0 wt% Na_2O, and 6.7–8.1 wt% K_2O. Conversely, cluster 2 follows a trend of decreasing MgO, CaO, and K_2O, and increasing Na_2O with increasing SiO_2. It occupies an almost identical range of SiO_2 contents as cluster 1, with 0.3–1.0 wt% MgO, 1.7–3.0 wt% CaO, 3.0–5.7 wt% Na_2O, and 7.9–10.8 wt% K_2O. Cluster 3, which has the highest SiO_2 content of all glass analyses, has a narrow range of 65.1–65.7 wt% SiO_2, 5.4–5.9 wt% Na_2O, and 6.4–6.8 wt% K_2O, and has MgO values of roughly 0.2 wt% and CaO values of roughly 1.5 wt%. Cluster 4 is less distinct in MgO/SiO_2, CaO/SiO_2, and K_2O/SiO_2 space and could be interpreted as representing more evolved points within cluster 1; however, its distinct Na_2O/SiO_2 ratio suggests an origin and/or history for cluster 4 that is disconnected from that of cluster 1. It has a range of 62.7–63.5 wt% SiO_2, 0.3–0.4 wt% MgO, 2.0–2.2 wt% CaO, 3.6–4.5 wt% Na_2O, and 7.7–8.7 wt% K_2O.

A mixture of cluster 1 and 2 values is found in the majority of ignimbrite samples. The PPF beneath the ignimbrite, by comparison, is only composed of materials found in cluster 1. Two samples taken from near the top of the proximal stratigraphy, C19-40d and CF323, conspicuously contain almost exclusively cluster 2 values. Cluster 3 is defined entirely by one sample, C19-1c (plus just one data point from C19-40d), and cluster 4 is defined entirely by data from sample C19-30d. Figure 5C shows the compositional clusters observed within each sample for proximal deposits and for the distal deposits overall.

The USAF, WGI, LYT, Piperno, LPFU, and BU in Fedele et al.'s (2008) scheme and Units A, B, and C in Rosi et al.'s (1996) scheme and the ultra-distal co-ignimbrite data all contain a substantial population of compositions within clusters 1 and 2. All samples analyzed within these units represented by more than two data points have data in both clusters, except for two samples of the USAF that only have cluster 1 data (C19-26d and CF344/CF346). The UPFU and Unit D, represented by the previously mentioned C19-40d and CF323 samples, have data almost exclusively in cluster 2. The LPFU and Unit B are the only units that have data in all four clusters; the two samples that define clusters 3 and 4, C19-1c and C19-30d, respectively, are both from exposures designated as LPFU by Fedele et al. (2008) and Unit B by Rosi et al. (1996). The WGI, BU/Unit C (at

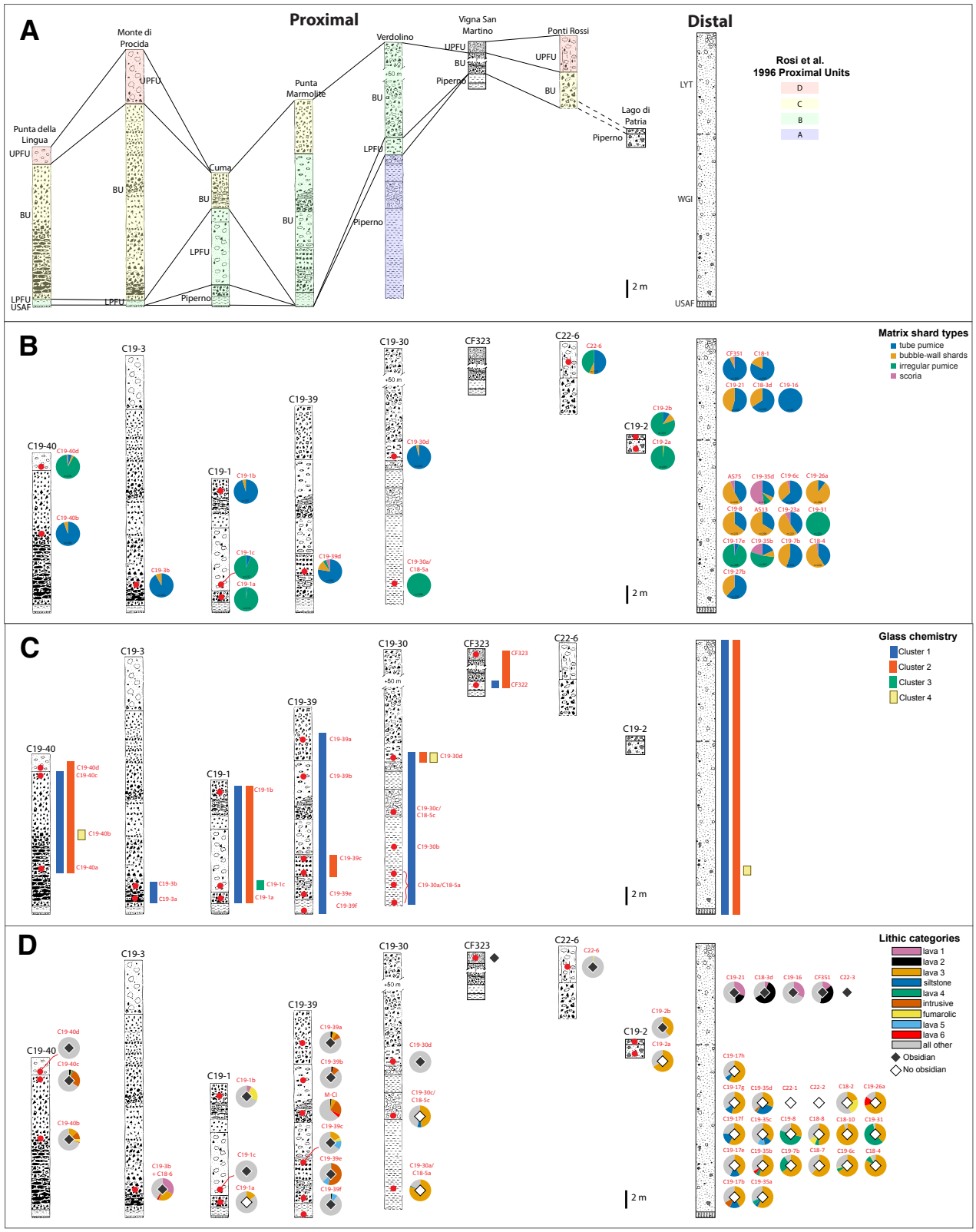

Figure 5. Stratigraphic columns adapted from Rosi et al. (1996) and Di Salvo et al. (2020) of all proximal exposures sampled and a composite schematic unscaled column for the distal deposits. (A) Units assigned by Rosi et al. (1996) to each exposure are shown with colored fill, and units assigned by Fedele et al. (2008) and Di Salvo et al. (2020) using Fedele et al.'s (2008) schema are shown with connecting lines. (B) Glass shard types found in each sample are displayed with pie charts beside their approximate sample locations. (C) Colored bars mark the presence of matrix glass compositions belonging to the four compositional clusters observed. Rough sampling heights within stratigraphy are marked. (D) Pie charts showing the predominance of correlating lithic types are marked adjacent to sample sites. Diamonds indicate the presence or absence of obsidian. All data for the distal deposits in panels B, C, and D are shown without stratigraphic heights marked on the generalized stratigraphic column, but samples collected in a vertical sequence are displayed in order.

TABLE 2. MATERIALS SAMPLED AND ALL ASSOCIATED DATA SETS

Sample	Location	Location code	Unit (Fedele et al., 2016)	Units (Rosi et al., 1996)	Latitude	Longitude	Obsidian	Dominant shard type	Glass composition	Lithic categories
AS13	Roccamonfina	AS13	WGI		41.289440	13.992780	n	bws	1	
C18-1	Tocco Caudio	C18-1	LYT		41.122173	14.626090	y	tp		
C18-10	Mortola	C18-10	WGI		41.349057	13.880445	n			lava 3
C18-2	Tufara	C18-2	WGI		41.059322	14.710237	n	bws		lava 3, fumarolic
C18-3a	Altavilla	C19-27	PPF		41.007110	14.765484	n			
C18-3a	Altavilla	C19-27	USAF		41.007110	14.765484	n			
C18-3b	Altavilla	C19-27	WGI		41.007110	14.765484	n			
C18-3c	Altavilla	C19-27	WGI		41.007110	14.765484	n			
C18-3d	Altavilla	C19-27	LYT		41.007110	14.765484	y	tp		lava 1, lava 2
C18-4	Monteforte Irpino	C18-4	WGI		40.914192	14.671415	n	bws		lava 3, lava 4, fumarolic
C18-7	Mondragone	C18-7	WGI		41.125180	13.910958	n	tp		lava 3, lava 4, fumarolic
C18-8	Mondragone	C18-8	WGI		41.307513	13.894811	n			lava 3
C19-14	Roccamonfina	C19-14	USAF		41.271652	13.994178	n	tp		
C19-16	Caserta	C19-16	LYT		41.063117	14.345212	y	tp		lava 1
C19-17b	Gradillo	C19-17	WGI		41.124016	14.337330	n	ip		lava 3, siltstone, intrusive
C19-17c	Gradillo	C19-17	WGI		41.124016	14.337330	n	ip		
C19-17d	Gradillo	C19-17	WGI		41.124016	14.337330	n	ip	1	
C19-17e	Gradillo	C19-17	WGI		41.124016	14.337330	n	ip		lava 3, siltstone
C19-17f	Gradillo	C19-17	WGI		41.124016	14.337330	n	ip		lava 3, siltstone
C19-17g	Gradillo	C19-17	WGI		41.124016	14.337330	n	ip		lava 3, siltstone
C19-17h	Gradillo	C19-17	WGI		41.124016	14.337330	n	ip		lava 3, siltstone
C19-1a	Cuma	C19-1	Piperno	B	40.848895	14.050261	n	ip	1,2	lava 3
C19-1b	Cuma	C19-1	BU	C	40.848895	14.050261	y	tp	1,2	lava 1, fumarolic, lava 5
C19-1c	Cuma	C19-1	LPFU	B	40.848895	14.050261	y	ip	1,2,3	none
C19-20	St Agata di Goti	C19-20	LYT		41.091604	14.511486	y			
C19-21	Capellino	C19-21	LYT		41.097464	14.486880	(y)	tp		lava 1, lava 2
C19-22	Bagnoli	C19-22	LYT		41.091132	14.447093	y			
C19-23a	Mellizano	C19-23	WGI		41.162706	14.501623	n	bws		
C19-23b	Mellizano	C19-23	WGI		41.162706	14.501623	n			
C19-23c	Mellizano	C19-23	WGI		41.162706	14.501623	n			
C19-24	Ruviano	C19-24	LYT		41.209694	14.407203	y			
C19-26a	Aqua Fidia	C19-26	WGI		40.929255	14.700284	n	bws	1	lava 3, lava 6
C19-26b	Aqua Fidia	C19-26	USAF		40.929255	14.700284	n	bws	1	
C19-26d	Aqua Fidia	C19-26	PPF		40.929255	14.700284	n	tp	1	
C19-27a	Altavilla	C19-27	WGI		41.008969	14.767951	n	tp	1,2	
C19-27b	Altavilla	C19-27	WGI		41.008969	14.767951	n	tp		
C19-27c	Altavilla	C19-27	WGI		41.008969	14.767951	n	tp		
C19-27d	Altavilla	C19-27	WGI		41.008969	14.767951	n	tp		
C19-27e	Altavilla	C19-27	WGI		41.008969	14.767951	n	tp	1	
C19-27f	Altavilla	C19-27	WGI		41.008969	14.767951	n	tp	1	
C19-27g	Altavilla	C19-27	WGI		41.008969	14.767951	n	tp	1	
C19-28	Tufara	C19-28	WGI		41.057471	14.708145	n			
C19-29	Tufara	C19-29	WGI		41.054712	14.679255	n			
C19-2a	Lago di Patria	C19-2	Piperno		40.933637	14.053977	n	ip		lava 3

(*Continued*)

TABLE 2. MATERIALS SAMPLED AND ALL ASSOCIATED DATA SETS (*Continued*)

Sample	Location	Location code	Unit (Fedele et al., 2016)	Units (Rosi et al., 1996)	Latitude	Longitude	Obsidian	Dominant shard type	Glass composition	Lithic categories
C19-2b	Lago di Patria	C19-2	Piperno/BU		40.933637	14.053977	y	tp		lava 3
C19-30 a f-h + C18-5 (1,3,5)	Verdolino	C19-30	Piperno	A	40.855242	14.207623	n	ip	1	
C19-30a b-h + C18-5 (2,4)	Verdolino	C19-30	Piperno	A	40.855242	14.207623	n	ip		lava 3, siltstone
C19-30b + C18-5b	Verdolino	C19-30	Piperno	A	40.855242	14.207623	n	ip		
C19-30c + C18-5c	Verdolino	C19-30	Piperno	A	40.855242	14.207623	n	ip		lava 3, siltstone
C19-30d	Verdolino	C19-30	LPFU	B	40.855242	14.207623	y	tp	1,2	none
C19-31	Castel San Giorgio	C19-31	WGI		40.779823	14.650882	n	ip		lava 3, lava 4
C19-32	Pucara	C19-32	WGI		40.676401	14.643780	n			
C19-33	Polvica	C19-33	WGI		40.694150	14.636413	n			
C19-34	Monticchio	C19-34	WGI		40.598796	14.354637	n			
C19-35a	Piano di Sorrento	C19-35	WGI		40.636582	14.401696	n	ip		lava 3, siltstone, lava 4, lava 5
C19-35b	Piano di Sorrento	C19-35	WGI		40.636582	14.401696	n	ip	1	lava 3, siltstone, lava 4, lava 6
C19-35c	Piano di Sorrento	C19-35	WGI		40.636582	14.401696	n	ip		lava 3, siltstone, intrusive, lava 5
C19-35d	Piano di Sorrento	C19-35	WGI		40.636582	14.401696	n	tp		lava 3, siltstone, lava 4, intrusive
C19-35e	Piano di Sorrento	C19-35	WGI		40.636582	14.401696	n			
C19-36	Fosso di Prepezzano	C19-36	WGI		40.697515	14.887023	n			
C19-37	Cologna	C19-37	WGI		40.721635	14.776368	n			
C19-39a	Punta Marmolite	C19-39	BU	C	40.896102	14.136869	y	tp	1	lava 2, lava 3, intrusive
C19-39b	Punta Marmolite	C19-39	BU	B	40.896102	14.136869	y	tp	1	lava 1, lava 2, intrusive
C19-39c	Punta Marmolite	C19-39	BU	B	40.896102	14.136869	y	tp	1,2	lava 3, intrusive, fumarolic, lava 5
C19-39d	Punta Marmolite	C19-39	BU	B	40.896102	14.136869	y	tp	1,2	
C19-39e	Punta Marmolite	C19-39	BU	B	40.896102	14.136869	y	tp	1	lava 4, intrusive, lava 5
C19-39f	Punta Marmolite	C19-39	BU	B	40.896102	14.136869	y	tp	1	lava 2, lava 4, lava 5
C19-3a	Monte di Procida	C19-3	SU	C	40.792688	14.043865	n	tp		none
C19-3b + C18-6	Monte di Procida	C19-3	BU	C	40.792688	14.043865	y	tp	1	lava 1, lava 3, intrusive, fumarolic, lava 6
C19-40a	Punta della Lingua	C19-40	SU	C	40.765020	14.035133	n			none
C19-40b	Punta della Lingua	C19-40	BU	C	40.765020	14.035133	y	tp	1,2	lava 3, intrusive, fumarolic, lava 6
C19-40c	Punta della Lingua	C19-40	BU	C	40.765020	14.035133	y	tp	1,2	lava 2, lava 3, lava 4, intrusive
C19-40d	Punta della Lingua	C19-40	UPFU	D	40.765020	14.035133	y	ip	2	none
C19-6c	San Lorenzello	C19-6	WGI		41.269727	14.531329	n	bws		lava 3, lava 4, fumarolic
C19-7b	Civitella	C19-7	WGI		41.310078	14.536603	n	tp		lava 3, lava 4
C19-8	Giano Vetusto	C19-8	WGI		41.202834	14.185550	n	bws		lava 3, lava 4
C22-1	Sant'Angelo in Formis	C22-4	WGI		41.107963	14.260030	n			
C22-2	Trifilsco	C22-2	WGI		41.137369	14.253170	n			
C22-3	San Nicola la Strada	C22-3	LYT		41.053457	14.344412	y			
C22-4	Viscone	C22-4	PPF		40.796994	14.657456	(y)			
C22-5	Zacharria	C22-5	UPFU	D	40.904012	14.093487	y			
C22-6	Ponti Rossi	C22-6	UPFU	D	40.875200	14.262818	y	tp		fumarolic
CF283	Monte di Procida	C19-3	LPFU	B	40.792688	14.043865				
CF290	Mondragone	C18-7	WGI		41.125180	13.910958				
CF317	Verdolino	C19-30	Piperno	A	40.855242	14.207623			1	
CF321	Vigna San Martino	CF323	PPF		40.843730	14.242920			1	
CF322	Vigna San Martino	CF323	Piperno		40.843730	14.242920			1,2	
CF323	Vigna San Martino	CF323	UPFU		40.843730	14.242920	y		2	

(*Continued*)

TABLE 2. MATERIALS SAMPLED AND ALL ASSOCIATED DATA SETS (*Continued*)

Sample	Location	Location code	Unit (Fedele et al., 2016)	Units (Rosi et al., 1996)	Latitude	Longitude	Obsidian	Dominant shard type	Glass composition	Lithic categories
CF324	Vigna San Martino	CF323	UPFU		40.843730	14.242920			2	
CF326	Monte di Procida	C19-3	BU	C	40.792688	14.043865			1	
CF327, CF329, CF331-CF346	Altavilla	C19-27	USAF		41.007110	14.765484			1,2	
CF328	Altavilla	C19-27	WGI		41.007110	14.765484			1,2	
CF330	Altavilla	C19-27	WGI		41.007110	14.765484			1,2	
CF332	Altavilla	C19-27	PPF		41.007110	14.765484			1	
CF342, CF343	Baiano	CF342	PPF		40.915480	14.667620			1	
CF344, CF346	Baiano	CF342	USAF		40.915480	14.667620			1	
CF350	Dugenta	CF350	LYT		41.122222	14.443889			1,2	
CF351	Dugenta	CF350	LYT		41.122222	14.443889	y	tp		lava 1, lava 2
CF352	Dugenta	CF350	LYT		41.122222	14.443889			1,2	
M-CI-1	Punta Marmolite	C19-39	BU	B	40.896102	14.136869				intrusive
M-CI-2	Punta Marmolite	C19-39	BU	B	40.896102	14.136869				lava 2, intrusive, lava 6
M-CI-3	Punta Marmolite	C19-39	BU	B	40.896102	14.136869				none
M-CI-4	Punta Marmolite	C19-39	BU	B	40.896102	14.136869				lava 3
RC9-189-1	Ionian seafloor	RC9-189-1	Co-ign		36.98	19.68		bws	1,2	
TR-172-12	Mediterranean seafloor	TR-172-12	Co-ign		33.90	29.26		bws	1,2	

Notes: n—none, y—yes, (y)—yes, very little, tp—tube pumice, bws—bubble-wall shards, ip—irregular pumice, BU—Breccia Unit, LPFU—Lower Pumice Flow Unit, LYT—Lithified Yellow Tuff, PPF—Plinian Pumice Fall, UPFU—Upper Pumice Flow Unit, USAF—Unconsolidated Stratified Ash Flow, WGI—Welded Grey Ignimbrite, co-ign—ultra-distal co-ignimbrite.

C19-40b), and co-ignimbrite all have a small number of data points in cluster 4, but only the LPFU has more than one data point in cluster 3.

3.3 Lithic Componentry and Obsidian

Accessory lithic clasts incorporated during eruption can be useful for understanding the basement geology of the vent region and can also be used to link proximal and distal units from the same vent (Hildreth and Mahood, 1986; Rosi et al., 1996). The lithic clasts observed within the Campanian Ignimbrite reflect the rock types present in the Campi Flegrei volcanic field prior to the formation of the caldera. The variety of rock types observed includes lavas and shallow intrusive rocks of various compositions, older lithified tuffs, clastic sedimentary rocks, fumarolic sublimates, and skarns, all of which vary from fresh to intensely altered.

The samples analyzed for this study contained 171 potentially distinct rock types. Most lithic types are only found within one of the defined units, and many are only found in a single sample and thus are not useful for correlation purposes. Nine lithic types that are sufficiently distinct to be tentatively tied to a single source each and that are found in both proximal and distal deposits are identified in Table 3. These nine rock types are used to consider potential connections between the proximal and distal deposits based on source vents. Although they make up a small minority of the total lithological variety, they make up the majority of the total quantity of lithic clasts in many outcrops.

Several distinct groups of samples can be distinguished based on the correlated lithic types. The first group consists of samples containing only lithic types referred to as lava 1 +/– lava 2, which together make up one-third or more of all the lithic clasts counted. These samples are all in the upper distal stratigraphy. The second group consists of samples containing only lava 3 +/– siltstone. These samples are all found near the bottom of the proximal stratigraphy. A third group consists of samples that contain none of the correlated lithic types. This group consists of sample C19-40d, an ash-rich exposure at the top of the proximal stratigraphy, and samples C19-1c and C19-30d, pumice-rich exposures lower in the stratigraphy. A fourth group can be defined for the remainder of the distal samples not in the first group, which are generally lower in the stratigraphy. More than 20% of the lithic content of each of these samples is lava 3, none of them contain any lava 1 or lava 2, and all of them have >44% correlated lithic clasts total. All but one of the remaining samples are from the proximal breccias. This set of samples, called group five by default, contains highly variable combinations of any of the correlated lithic types and is generally dominated by a wide variety of uncorrelated lithic types. The single sample that does not fit well into any group is from C22-6, which is found at the top of the proximal stratigraphy (assigned to the UPFU

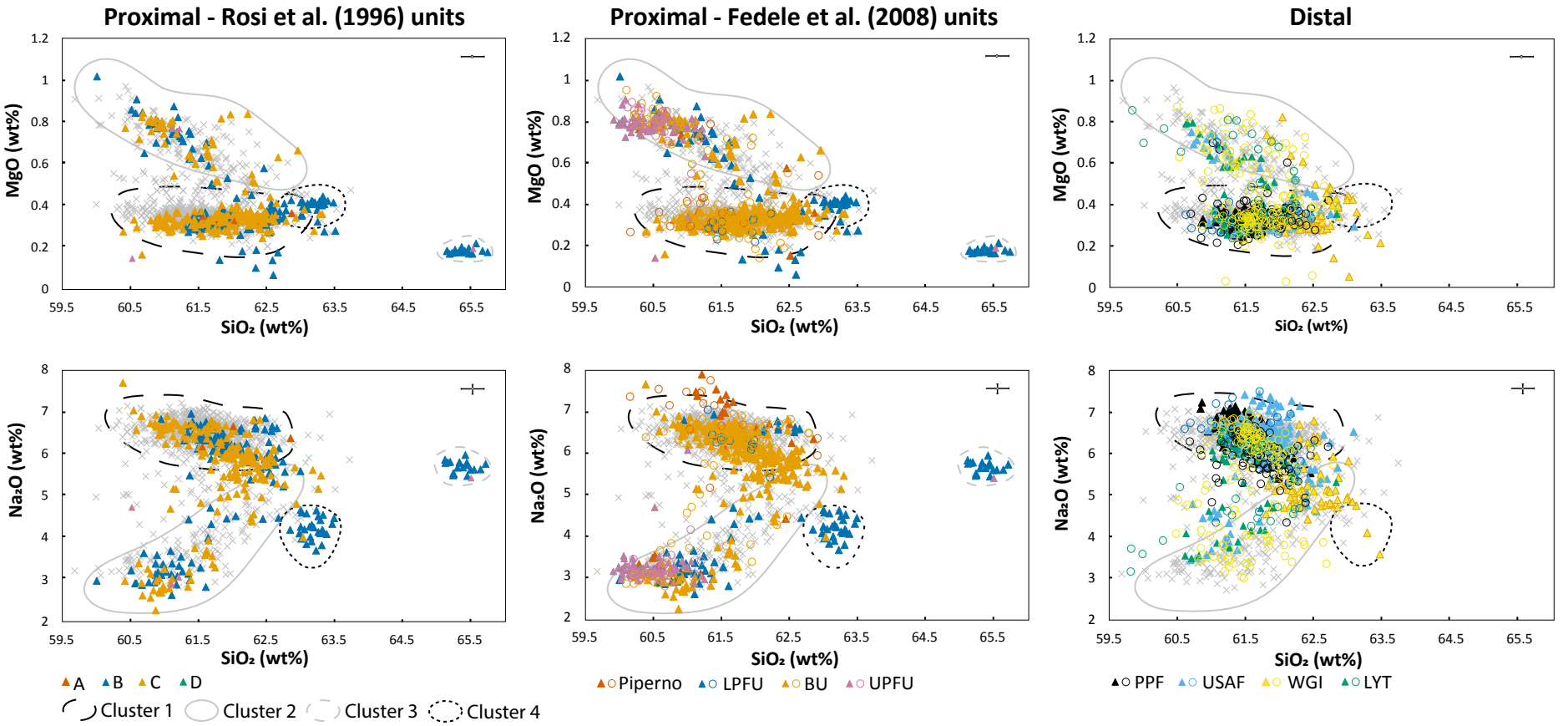

Figure 6. Harker plots showing major element compositions of ignimbrite and co-ignimbrite matrix glass for all units. Empty circles represent data from the literature (Melluso et al., 1995; Civetta et al., 1997; Fulignati et al., 2004; Fedele et al., 2016; Smith et al., 2016; Di Salvo, 2018). Light gray Xs on every graph give co-ignimbrite glass compositions from Wagner et al. (2008), Vogel et al. (2009), Caron et al. (2010), Damaschke et al. (2013), Cullen et al. (2014), Matthews et al. (2015), and Smith et al. (2016). Each data point plotted represents a single glass analysis. Shapes show compositional clusters: black dashes—cluster 1, gray line—cluster 2, gray dashes—cluster 3, and black dots—cluster 4. An indicator of average error bars from microprobe error is provided for all plots.

or Unit D). It contains a very small amount of fumarolic material and is otherwise dominated by uncorrelated lithic types (Fig. 5D).

Lithic groupings 1 and 4 correspond exactly to the LYT and WGI, respectively; the two previously described distal units have completely distinct lithic types. Group 2 samples are all samples of the Piperno and Units A or B in the proximal deposits. Group 3 includes both samples of LPFU (Unit B) and one sample of UPFU (Unit D). The other sample of UPFU/Unit D is the sample that does not belong to any group. Group 5 consists of all samples of the BU and Unit C and some from Unit B (Fig. 7). No overall patterns in the distribution of lithic types, including correlated and uncorrelated types, are discernible within any unit, either with respect to spatial distribution or height within a section.

Obsidian is observed in the upper portions of the stratigraphy wherever they are exposed and absent in the lower portions (Fig. 5D). It is found in the

TABLE 3. PERCENTAGE OF LITHIC CLASTS IN EACH UNIT THAT BELONG TO THE NINE CORRELATED LITHIC TYPES

Name	Type	Description	Proximal (% of clasts)								Distal (% of clasts)	
			Piperno	LPFU	BU	UPFU	A	B	C	D	WGI	LYT
Lava 1	2	Off-white to grey-tan, irregular coloration, subrounded–subangular irregular and lumpy shape, poorly sanidine-phyric, glassy lava			5			0.1	9			27
Lava 2	3	Off-white, subrounded, poorly coarse sanidine-phyric with smaller black phenocrysts, glassy lava			1			1	1			15
Lava 3	8	Grey to very fine salt-and-pepper, angular to subrounded, rarely poorly clinopyroxene- or sanidine-phyric, rare voids, finely crystalline to microcrystalline lava	52		8		57	6	8		51	
Siltstone	9	Light yellow, green and grey-brown, angular to subangular, well-sorted siltstone	3				5				7	
Lava 4	10	Grey, subrounded–angular, poorly sanidine and clinopyroxene-phyric, poorly to moderately vesicular, yellow alteration inside vesicles, microcrystalline–glassy lava			0.4			0.4	0.2		8	
Intrusive	11	Light grey to tan, angular, crystalline, inequigranular, few have slight fabric, brown and yellow alteration concentrated around rare angular voids, intrusive			13			13	7		1	
Fumarolic	12	Off-white or pastel, black specked, rounded to subangular, few embedded crystals, powdery–granular, fumarolic			4	1		1	6	1	2	
Lava 5	13	Black and grey to brown banded, poorly sanidine- and clinopyroxene-phyric, lighter bands are finely vesicular, glassy lava			4			6	0.2		1	
Lava 6	14	Light grey and white, banded to streaky, subangular, some poorly sanidine- and clinopyroxene-phyric, poorly to moderately finely vesicular, more vesicles in lighter bands, glassy lava			1			0.4	1		1	
All other			45	100	64	99	38	73	69	99	30	58

Notes: BU—Breccia Unit, LPFU—Lower Pumice Flow Unit, LYT—Lithified Yellow Tuff, UPFU—Upper Pumice Flow Unit, WGI—Welded Grey Ignimbrite.

form of angular, black glassy clasts of a similar size to the lithic clasts in each exposure; some larger pieces contain feldspar phenocrysts. It is unaltered and easily distinguishable in color and texture from spatter and fiamme. Obsidian is observed in all samples of the LPFU, BU, UPFU, and LYT, and is absent from the PPF, USAF, WGI, and Piperno exposures. The transitional Piperno/BU sample, C19-2b, contains obsidian. Correspondingly, in the Rosi et al. (1996) scheme, Unit A lacks obsidian and Unit D contains it, but Units B and C are inconsistent.

4. DISCUSSION

4.1 Interpretations

4.1.1 Matrix Componentry

The matrix component assemblage of the Campanian Ignimbrite is distinct in different portions of the deposits but has no simple relation with the previously defined stratigraphic schemes. The distinctive clast-supported lithic breccias of the proximal deposits, which are called the BU by Fedele et al. (2008) and Unit C by Rosi et al. (1996), have predominantly tube pumice in their matrix ash. They share this in common with the LYT, which is the upper portion of the distal deposits wherever it is observed. Deposits above the proximal lithic breccias, which are assigned to the UPFU and Unit D, have irregular-pumice–dominated matrix ash. Fiamme-rich and lithic-rich welded ignimbrite deposits at the base of the proximal deposits, including the Piperno, Unit A, and parts of Unit B, are also dominated by irregular pumice. Pumice-rich exposures below the BU, which are assigned to the LPFU and parts of Unit B, can be dominated by either of these matrix types. Exposures of the non-lithified ignimbrite that makes up most of the Campanian Ignimbrite's volume, generally assigned to the WGI, can have one of three different matrix types, including the tube-pumice and irregular-pumice–dominated types observed in the proximal deposits, and a third type dominated by larger bubble-wall shards.

Some overall patterns appear in the spatial distribution of matrix types within the exposures assigned to the WGI, but several outliers are noted. Generally, irregular-pumice–dominated matrix is found in exposures that are closer to the caldera near the ventward base of the first major topographic obstacle that the PDCs encountered on a given trajectory. The tube-pumice–dominated matrix type is found in the most distal exposures but also in one less distal exposure (roughly 39.5 km from the center of the caldera) on the Campanian plain (C18-7 in Fig. 1). The percentage of tube-pumice shards generally increases away from the caldera in any given direction. The two highest elevation exposures (C19-26 and AS13 in Fig. 1) have the highest percentages of bubble-wall shards, but four other exposures within the Apennines are also bubble-wall-shard dominated to a lesser degree. The ultra-distal co-ignimbrite samples analyzed for comparison are the most bubble-wall-shard dominated of all. This may point to a stratification of shard types within the PDCs, with more bubble-wall shards concentrated in the low-density upper portion of the PDCs from which the high-elevation exposures were deposited (Fisher et al., 1993; Ort et al., 2003) and from which the co-ignimbrite ash column should have been generated (Woods and Wohletz, 1991; Gardner et al., 2017a). The

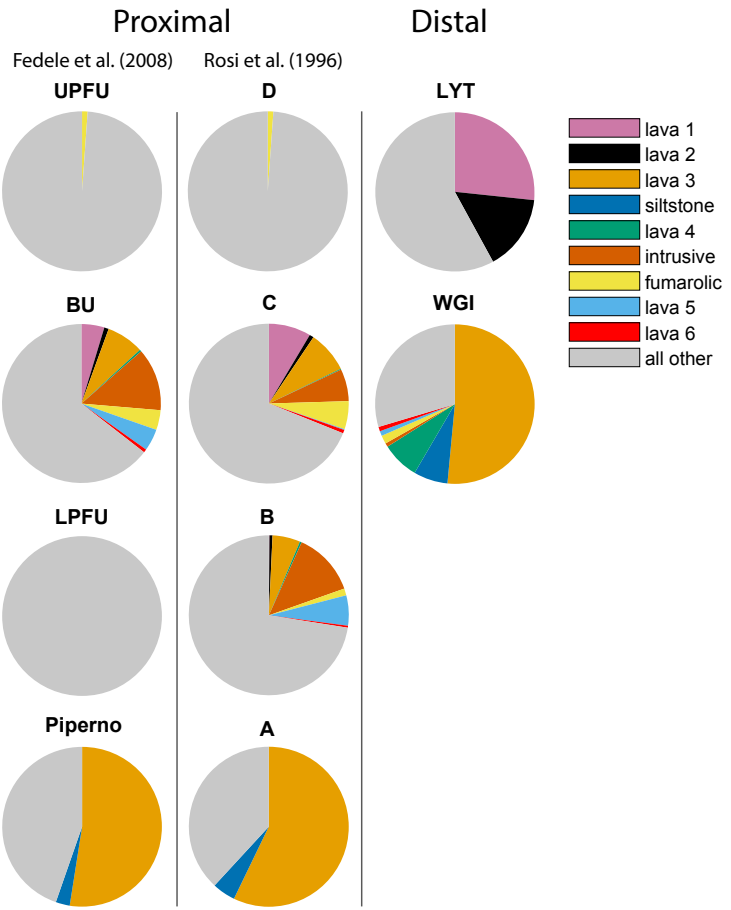

Figure 7. Pie charts showing the prevalence of the nine correlated lithic types found in each proximal and distal unit. UPFU—Upper Pumice Flow Unit; BU—Breccia Unit; LPFU—Lower Pumice Flow Unit; LYT—Lithified Yellow Tuff; WGI—Welded Grey Ignimbrite.

absence of significant quantities of bubble-wall shards in more proximal outcrops and their prevalence in the most distal and highest elevation deposits, deposited by the most mobile portions of the current, supports a model of early near-vent inflation of the PDCs driven primarily by magmatic gas. This is consistent with observations of high-emplacement temperatures throughout the ignimbrite (Ort et al., 2018; Silleni, 2019).

The three dominant types of matrix shards may shed light on the dominant conduit processes that occurred at different times during the eruption. Polacci et al. (2003) proposed that increases in the quantity of tube-pumice clasts within the fall stratigraphy were the product of either increased velocity gradients along conduit walls producing more sheared vesicles accompanied by increased conduit erosion, or an increase in the total amount of conduit-wall surface area. In this framework, the portions of the ignimbrite that are tube-pumice–shard dominated, including all exposures of the LPFU, BU, and LYT and some exposures of WGI, may record eruptive phases with high shear within the conduits and/or conduits with irregular and elongate shapes maximizing surface area. The irregular pumice shards would therefore predominate during eruptive phases with less conduit erosion and lower shear. The bubble-wall shards are the walls of vesicles much larger than those seen in the other shard types and in the pumice lapilli of the ignimbrite. The larger bubbles preserved in this shard type could have been generated by expansion or coalescence (Klug and Cashman, 1996). This could also support the idea that they are connected to eruptive phases with high concentrations of magmatic gas. The shards may be related to the expanded pumice clasts described by Polacci et al. (2003) in the PPF, observed at outcrop C22-4. Whether reduction to ash-sized particles occurred primarily in the conduit as the result of fragmentation or as the result of abrasion in the flow is impossible to discern from our data. Expanded pumice clasts are more fragile than other clast types and would fragment and abrade during transport within a PDC, making them rare within the lapilli of the ignimbrite, but bubble-wall shards of ash size, on the scale of the vesicles, would remain. Both low-density pumice with larger vesicle sizes and the individual bubble-wall shards with their irregular to flat shapes may have a lower settling velocity than other juvenile clasts of equivalent size (Dioguardi et al., 2017; Mele and Dioguardi, 2018; Saxby et al., 2018) and thus may be more likely to stay in the transport system rather than falling into the depositional system of the PDCs. This could also contribute to the greater prevalence of bubble-wall shards at high elevation and in the co-ignimbrite deposits.

4.1.2 Major-Element Chemistry

Major-element chemistry of the proximal and distal deposits of the Campanian Ignimbrite show four general geochemical populations, with two of these being dominant. Most of the previously defined units have data distributed across the two major populations. Thus, major-element chemistry does not serve to distinguish any of the proximal and distal deposits as definitively connected (or not) to one another. The only units that are distinctive are the PPF, the pumice fall deposited before the ignimbrite (not part of the ignimbrite), which has data only in one of the two main clusters (cluster 1 in Fig. 6), and the UPFU/Unit D, with data almost exclusively in the other main cluster (cluster 2 in Fig. 6). The LPFU/Unit B is also unique because it includes two minor geochemical populations (clusters 3 and 4, which are each found only in single samples) in addition to having data in the two main populations. All materials stratigraphically above the PPF and below the UPFU in the proximal deposits contain glass in both clusters 1 and 2.

The major-element chemistry observed in this study is partially compatible with the model for the Campi Flegrei magmatic system proposed by Arienzo et al. (2009, 2011) and Pabst et al. (2008) of a two-magma system composed of a less-evolved trachyte that intruded into more-evolved trachyte from a reservoir at greater depth. The two dominant glass compositions that we observe (clusters 1 and 2) consist of two trachytes showing distinct evolutionary histories, with the more evolved trachyte erupting first (as the PPF). The two distinct glass compositions, which occur in all deposits between the PPF and UPFU, indicate that mixing between the two dominant compositional populations was very limited, and, instead, that two magmas, which do not appear to be related by any late-stage fractionation process, erupted simultaneously. The two minor geochemical components (clusters 3 and 4) observed in the LPFU are not accounted for in the model proposed by Arienzo et al. (2009, 2011) because the LPFU was not sampled for those studies.

Our findings do not support a simple pattern of the progressive eruption of less-evolved compositions with time, which has been proposed as the product of: (1) a compositionally stratified single magma chamber, with the more-evolved trachyte stored atop the less-evolved trachyte (Civetta et al., 1997; Fedele et al., 2016; Forni et al., 2016), or (2) a vertically or concentrically zoned single magma chamber (Signorelli et al., 1999). The two main magma compositions do not appear to be related to one another by simple fractional crystallization (Di Salvo et al., 2020), which suggests physically separate batches of magma stored at depth. This hypothesis is also supported by the isotopic data of Pappalardo et al. (1999) and Pabst et al. (2008). Additionally, this study found no pattern of compositional change vertically or laterally within any of the units. Civetta et al. (1997) described a trend within the distal deposits of less-evolved compositions being found closest to the caldera and the most evolved compositions being found in the western sector of the Campanian plain. Fedele et al. (2016) described a trend of increasingly less-evolved compositions in the WGI both upward in the deposits and with distance from the caldera (thus opposite to Civetta et al., 1997). Our data set does not align with either of these patterns, but it does not preclude the possibility of there being some geographic controls on average composition. Differences in the range of compositions observed at exposures sampled by different studies may be the result of different data filtration methods and small glass chemistry sample sizes.

4.1.3 Lithic Componentry and Obsidian

Lithic-clast componentry shows correspondence among the proximal and distal deposits but no unique connections between the units of either stratigraphic scheme, and no indication of vertical or lateral patterns within the distal deposits. The upper and lower distal deposits, the LYT, and WGI share a lithic type with the proximal lag breccias (BU/most of Unit C), but they do not share lithic types with each other. The WGI also shares some dominant lithic types with the welded lithic- and fiamme-rich deposits at the base of the proximal stratigraphy—the Piperno, Unit A, and some of Unit B. The ash- and pumice-dominated horizons of the proximal deposits, including the LPFU, UPFU, and parts of Units B and D, generally do not share lithic types with the distal deposits.

Lithic componentry in an ignimbrite is primarily representative of the rock types intersected by the conduit at the depth of fragmentation throughout the eruption (Hildreth and Mahood, 1986; Suzuki-Kamata et al., 1993; Pittari et al., 2008). Accidental lithic clasts picked up during overland flow also occur in many ignimbrites. In the case of the Campanian Ignimbrite, the underlying rock units, where rock may have been exposed at the surface at the time of the eruption, are limestone in the Appenines and older Campi Flegrei volcanic materials in the proximal areas. Outsized, poorly rounded clasts of limestone have been observed in a limited number of outcrops (Ort et al., 2003), but none were sampled in this study. It is not possible to distinguish which volcanic lithic types were excavated from the subsurface and which were picked up at the surface in the proximal areas. However, as a tool for correlation between proximal and distal outcrops, the difference becomes irrelevant, and during a caldera collapse scenario, potentially ambiguous. The very limited variety of lithic clasts found within the Piperno may indicate that it erupted from a limited number of vents at stable fragmentation depths. At the other extreme, the lithic diversity of the lag breccia, both within and between exposures, is consistent with its eruption from multiple vents that supplied lithic clasts from a variety of depths for lag-breccias deposited in their local areas. Laterally extensive rock units in the subsurface may have been intersected by several conduits and erupted from several vents, while local units may have been erupted from only one vent. The LPFU and UPFU, have low lithic content compared to the Piperno and BU, but their lithic content is extremely heterogeneous, which suggests the involvement of multiple vents. The wide variety of lithic types is reflective of the existence of numerous volcanic deposits, particularly domes and lava flows in the Campi Flegrei volcanic field prior to the formation of the caldera.

Obsidian is present in the upper portion of the stratigraphy, including the LPFU, BU, UPFU (Units B–D), and LYT, and absent from the lower part of the stratigraphy, including the PPF, USAF, Piperno (Units A and B), and WGI. Obsidian clasts are especially abundant in the BU, which contains blocks of up to approximately half a meter in diameter (Melluso et al., 1995; Rosi et al., 1996; Gebauer et al., 2014). The presence of obsidian, like the lithic componentry, is a product of the subsurface materials that were being sampled by conduit erosion. Compositional analysis by Fulignati et al. (2004), Fedele et al. (2008), and Forni et al. (2016) indicates that the obsidian is a juvenile material with compositions within cluster 1. This obsidian may have formed as part of domes or plugs during an early stage of the eruption or developed along conduit margins as a result of the sintering of glass and melt fragments to the conduit wall (Dunbar and Kyle, 1992; Gardner et al., 2017b). The appearance of obsidian partway through the stratigraphy of the Campanian Ignimbrite may be representative of a transition to increased conduit erosion, the widening of vents, and break-up of caldera blocks that resulted in the fragmentation and excavation of material emplaced earlier in the eruption (Vinkler et al., 2012). The deposits suggest that this transition occurred between the eruption of the

Piperno and LPFU or BU at different locations in the proximal deposits and between the WGI and LYT in the distal deposits.

4.2 Synthesis

The combined results of all lines of evidence in this study cannot be used to uniquely correlate any established proximal unit with any distal unit. Only one of the criteria we studied delineates a clear boundary in the stratigraphy that is observable in both the proximal and distal deposits: the presence or absence of obsidian. The lower ignimbrite units, the WGI in the distal areas, and the Piperno (Unit A and parts of Unit B) in the proximal area do not contain obsidian, while all units higher in the sequence, the distal LYT and proximal LPFU, BU, and UPFU (parts of Unit B, and Units C and D) do contain obsidian. This obsidian transition is the most significant boundary that we observed in the stratigraphy. The boundary establishes a connection between the WGI and Piperno, but this is not necessarily an exclusive or unique correlation. The WGI has a wider variety of lithic and matrix types, which indicates that the Piperno only correlates to a portion of the WGI.

Less definitive correlations are suggested based on other criteria. The dominance of cluster 2 glass compositions in the UPFU (Unit D) exposures that we sampled, relative to all other samples, seems to rule out a correlation between those exposures and anything in the distal deposits. However, we acknowledge that, given the heterogeneous nature of the UPFU exposures, this may not be true of all exposures. Both the UPFU and LPFU share a lack of common lithic types with the distal deposits and a lack of common shard types with the LYT. These characteristics indicate that they likely have no distal correlatives. The dominance of tube-pumice glass shards in the BU (Unit C and some of B) and LYT are suggestive of a connection between those units. However, tube-pumice shards are also dominant in some WGI exposures and are present in some proportion in the exposures of most units, so this does not define a unique connection. Our data suggest a connection between the Piperno and WGI and between the BU and LYT, but not exclusive correlations.

Comparison of the characteristics of the proximal exposures and bulk samples studied reveals substantial heterogeneity among exposures, not only in what units are present at each location, but in the characteristics of deposits identified as belonging to the same unit. At the outcrop, hand sample, and microscopic scales, there is substantial variability in deposit characteristics among materials assigned to the same unit. In the schema of Rosi et al. (1996), Unit B is so broadly defined as to be impossible to identify. This unit includes everything from clast-supported lithic breccias to pumice-dominated beds to ash-dominated layers and exposure both above and below the obsidian transition, which is the one universally defined correlative feature we found. The schema of Fedele et al. (2008) is more coherent in its subdivision of the deposits into four parts that align with the transitions described in the previous two paragraphs and can, in most cases, be distinguished in the field. However, the wide range of deposit characteristics and stratigraphic positions among outcrops assigned to the same unit are noteworthy. For example, the different exposures of the LPFU differ in matrix shard types, average grain size, consolidation, lithic componentry, sorting, structure, thickness, and color. The main similarities among the deposits are that they are all pumice- or ash-dominated and non-welded, traits they also share with much of the UPFU. The BU is the most recognizable unit and is consistently a clast-supported lithic breccia, but it is interbedded with other types of ignimbrite materials in places. At outcrop C19-39, for example, horizons of matrix-supported ignimbrite with coarse pumice clasts and few lithic clasts are interbedded with the lithic breccia; these horizons vary in number and thickness throughout the exposure area. The term Upper Pumice Flow Unit (or UPFU) is generally assigned to any proximal deposit found above the lag breccia in the proximal sequence, but the different outcrops assigned to this unit range from extremely ash-dominated, to pumice-rich with dense scoria and a high percentage of lithic clasts, to a deposit that resembles the LYT with larger pumice and lithic clasts. We therefore suggest that, while the four categories of Piperno, LPFU, BU, and UPFU are all useful subdivisions of the proximal deposits of the Campanian Ignimbrite, they are not subdivisions of equal stratigraphic significance.

We suggest the following conceptualization of the proximal stratigraphy regarding the Fedele et al. (2008) classifications. The Piperno's upper bound corresponds to the obsidian boundary, which gives this unit some chronostratigraphic significance in addition to being a lithostratigraphic unit. The Piperno consists of two lithofacies at the mesoscale that are generally identifiable in the field. The BU is the most easily distinguishable unit of the proximal sequence; it consists of a single lithofacies, but its emplacement was very likely not contemporaneous at all locations. The LPFU and UPFU are both collections of low-mobility PDC deposits and can be considered as very broadly defined depositional facies, but they are not lithofacies. They are distinguished from one another only by their positions in the stratigraphy (below and above the BU) and glass chemistry. Neither of these units could be classified as a real lithostratigraphic unit, but they are convenient collections of deposits that have low-mobility characteristics and do not belong to the Piperno or BU/SU.

The distal deposits have traditionally been divided into the WGI and LYT; the CPF, which we did not identify, is proposed to be above one or both at a few outcrops (Cappelletti et al., 2003; Sparice, 2015; Fedele et al., 2016). The WGI and LYT were considered by some to be distinguished only by alteration facies: gray feldspathized (not welded as the name suggests) and yellow zeolitized, respectively (Cappelletti et al., 2003; Langella et al., 2013; Fedele et al., 2016). We observe that WGI and LYT outcrops can also be distinguished based on differences in lithic componentry, shard shapes, and obsidian content. The WGI lacks obsidian and contains lithic-type lava 3 at all outcrops. The LYT contains obsidian and lithic-types lava 1 and lava 2 and has tube-pumice shards for matrix glass in every outcrop. Additionally, not all exposures of the distal Campanian Ignimbrite can be classified based on alteration facies. For example, the exposure at C19-22 is lithified but tan in color, C19-21 and C18-4 are yellow but non-lithified, C19-20 is brown and seems partially lithified, C19-35

grades upward from gray to tan-yellow and is indurated but non-lithified throughout, and C22-1 shifts from gray to yellow laterally within the same stratigraphic horizon and is non-lithified. These outcrops, which lack the typical color-based alteration facies, can still easily be assigned to a unit using the criteria developed in this paper. The presence of obsidian is particularly useful for rapid identification in the field. Based on lithic componentry and the presence of obsidian, C19-20, C19-21, and C19-22 are assigned to the LYT, and C19-35, C22-1, and C18-4 are assigned to the WGI. The fact that these sets of exposures were assigned correctly to the LYT and WGI in some existing literature (Sparice, 2015; Fedele et al., 2016) suggests that, in the absence of the dominant alteration facies characteristics, other criteria, perhaps similar to those used in this study, were used to subdivide the distal deposits, but these criteria have not been explicitly stated. We therefore assert that at most outcrops, the WGI and LYT can be primarily identified as lithofacies and secondarily as alteration facies.

Neither the proximal nor the distal deposits provide a complete record of the Campanian Ignimbrite eruption. Pumice-rich beds in the proximal deposits assigned to the LPFU or the UPFU do not have any stratigraphic equivalent in the distal deposits. This is likely because they were the product of low-mobility currents and limited in distribution. The observed exposures of the proximal deposits also do not record all of the eruptive products and processes within the eruption. Lithic types and shard types found in the distal deposits are absent from the proximal stratigraphy we sampled. This may be the result of a combination of insufficient sampling to cover the full diversity of proximal deposits; processes that transported materials such as bubble-wall shards, into the distal areas preferentially; and a genuine lack of proximal deposits representing the products of certain vents or certain periods within the eruptive sequence. This latter option could be due to non-depositional flow behavior (bypassing), erosion of deposited materials, and/or inconsistent activity of different vents. The proximal deposits are not laterally continuous nor laterally homogeneous but instead are highly heterogeneous and mostly found on the sides of paleohills, generally facing the caldera. The proximal deposits preferentially include, as can be expected, deposits of the lowest mobility phases, which travelled short distances and are influenced by topography, as well as the densest and coarsest materials from high-energy phases. We propose that the deposits observed at any proximal exposure are controlled primarily by what occurred at the vents closest to that location, and deposit characteristics cannot be easily generalized to exposures in other areas of the proximal deposits. For this reason, no proximal outcrop contains material derived from the entire duration of the eruption, and no outcrop is individually equivalent to the entire distal sequence. A corollary of this is that portions of the PDCs dominantly fed by different vents that were concurrently active would contribute different characteristics to the material that they deposited in distal areas. PDC lobes carrying different lithics, ash types, and other materials might arrive and deposit material in the same distal location at the same time after passing around topographic barriers and thereby mix materials derived from separate vents into one deposit.

We suggest that the Campanian Ignimbrite PDCs were substantially non-depositional in the proximal areas. In addition to the preferential deposition of dense materials and from less mobile currents in the proximal areas, it is also possible that significant quantities of proximal material deposited initially were removed by later eruptive phases, which behaved erosively for variable distances. Erosive basal contacts were observed below the BU, WGI, and USAF in this study at C19-39 and at various sites by Scarpati and Perrotta (2012). This supports the idea that the PDCs were occasionally erosive, at least in the places where they eventually left a deposit. Taken together, the results of all lines of analysis in this study allow different eruptive phases to be distinguished but do not point to a direct exclusive correlation of any previously established proximal unit with any distal unit.

4.3 Eruptive Model

Changes in the deposit characteristics analyzed in this study within the stratigraphy may be interpreted together to track how eruptive processes, magmatic sources, and vent characteristics evolved throughout the eruption. The transition from the dominance of irregular shards to tube-pumice shards, from the absence to the presence of obsidian, and from deposits with low-lithic diversity to high-lithic diversity occurs simultaneously between the Piperno and LPFU in the proximal deposits. In the distal deposits, the transition in shard shapes is within the WGI, and the lithic and obsidian transition is between the WGI and LYT. These characteristics suggest a possible change in shear in the conduits and increases in conduit erosion, respectively. Conduit erosion transitioned into conduit wall collapse during eruption of the BU, which consists largely of great quantities of excavated accessory material and obsidian. Together, these properties may be inferred to indicate the onset of caldera collapse, possibly preceded by diking along incipient caldera fractures that were chilled at shallow levels and later excavated as obsidian clasts (Vinkler et al., 2012). The formation of new elongate vents along ring fractures, between caldera blocks, and extending outward from the caldera would produce new and irregular conduit surface areas, thereby increasing shear, and greater and more varied areas of conduit wall failure. The introduction of two minor magmatic compositions during the eruption of the LPFU deposits is further evidence in line with the idea that new vents in and around the caldera began opening at this stage of the eruption. In a complex magmatic system, minor magmatic bodies could have been briefly tapped as new fractures opened.

Our proposed eruptive model, which expands on previous data and interpretations, is as follows:The eruption began with a Plinian column depositing the PPF at the base of the sequence. One magmatic composition was tapped for this phase of the eruption, and there was likely a single central vent. The nature of the USAF, next in the sequence, is poorly known and was not the focus of this study. The heterogenous appearance of its exposure and variable thickness relative to distance from the caldera, and its presence at the base

of the sequence in contact with several different lithofacies of the proximal deposits, may indicate that it is a depositional facies produced from the head of the first major PDC whenever it began to be deposited at a given location (Scarpati et al., 2015b).

The next major phase of the eruption appears to have emplaced the Piperno and the WGI. This was the most voluminous phase of the eruption, and the eruptive material was emitted from mostly stable conduit and vent systems that possibly consisted of one or more elongate fractures. During this phase, the second magma also began erupting, with both magmatic compositions being tapped simultaneously. The greater diversity of lithic and shard types in the WGI compared to the Piperno suggests that the Piperno exposures represent a limited subset of the eruptive vents and conditions associated with this phase overall. The idea that the most voluminous phase of the eruption occurred before the collapse of the caldera was suggested by Fedele et al. (2016), who proposed that the entirety of the distal deposits could be correlated with the Piperno. This might have been made possible at Campi Flegrei by the exploitation of preexisting regional faults within and around the caldera area (Vitale and Ciarcia, 2018) as a pathway for the release of eruptive products and by the unusually flexible nature of the rock materials within the caldera roof (Vanorio and Kanitpanyacharoen, 2015).

The LPFU began to be emplaced just before or at the beginning of the caldera collapse, as new vents—including potential ring fractures—were beginning to open. Lower pumice flow unit deposits are derived from low-mobility PDCs that erupted from a variety of vents within and near the caldera and potentially tapped several different magmatic bodies, including smaller melt pockets that were probably used up or not extracted further after this phase. The emplacement of the LPFU may have substantially overlapped in time with the emplacement of the BU from other vents. The main phase of caldera collapse resulted in the production of the lag-breccias of the BU and probably simultaneously the material that produced the LYT distally. The SU is interfingered with the BU in most locations where it appears. Based on the low-energy nature of spatter and the total lack of correlation of the lithic types within the two observed SU deposits, the SU is thought to be a very localized facies that requires the presence of nearby vents. Finally, the UPFU erupted, likely from a variety of vents, as the caldera blocks settled into place and the last of the eruptible magma was drained.

Thus, the Campanian Ignimbrite may be considered to have four major phases: (1) the Plinian Fall (Fig. 8A); (2) the pre-collapse phase, which is characterized by the eruption of homogeneous deposits from a limited set of vents (the proximal Piperno and distal WGI; Fig. 8B); (3) the syn-collapse phase, which is characterized by the eruption of heterogeneous deposits from a variety of vents (the LPFU, BU, SU proximal units, and the distal LYT; Fig. 8C); and (4) the late- or post-collapse phase (UPFU; Fig. 8D).

The eruption of these phases was probably continuous, as no evidence of significant time gaps is recorded in the stratigraphy. Pre- and syn-collapse facies might have been generated simultaneously in different areas of the caldera if the collapse were substantially uneven.

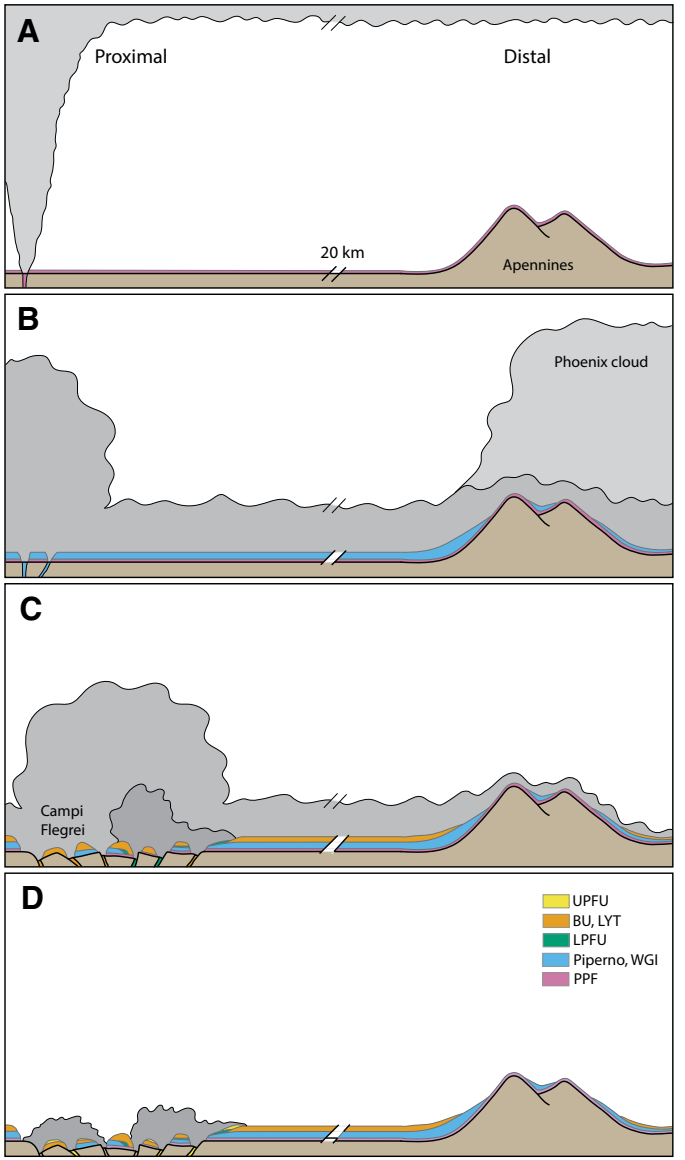

Figure 8. Schematic diagrams showing the four proposed eruptive phases for the Campanian Ignimbrite eruption and the units associated with them in the deposits. Colors shown inside the vents are intended to suggest the units that materials being erupted from those vents will form. Not to scale. UPFU—Upper Pumice Flow Unit; BU—Breccia Unit; LPFU—Lower Pumice Flow Unit; LYT—Lithified Yellow Tuff; PPF—Plinian Pumice Fall; WGI—Welded Grey Ignimbrite.

5. CONCLUSIONS

The Campanian Ignimbrite is an enigmatic ignimbrite that was deposited from a highly dilute and energetic PDC eruption at ca. 39.8 ka. The sporadic distribution of exposures, combined with the pronounced differences in the appearance of the proximal and distal deposits, have made developing a model for the stratigraphy of this ignimbrite a challenge. The shard shapes, types of lithic clasts, and glass chemistry do not define unique correlations among the previously defined stratigraphic units of the ignimbrite. These data do, however, provide evidence of important transitions in eruptive behavior that can be correlated across the proximal and distal deposits. Based on these associations, the eruption can be divided into four main phases: (1) an initial Plinian phase; (2) a pre-collapse phase that emplaced the proximal Piperno and the distal WGI; (3) a syn-collapse phase, when the proximal LPFU, BU, and SU and distal LYT were deposited; and (4) a post-collapse phase that produced the proximal UPFU. The stratigraphic variability of the proximal deposits and the absence of exclusive and complete correlations is evidence of complex eruptive processes with strong local influences. A combination of lab and field techniques made it possible to piece together the dynamics of the emplacement of the various deposits related to this eruption. This integrative method could be used in other complex eruptions where proximal deposits do not seem to correlate with distal equivalents.

ACKNOWLEDGMENTS

Funding was provided by the National Science Foundation (grant no. EAR1761713) to M.H. Ort, A. Silleni, and R.I. Gallo. R.I. Gallo was also supported by the Geological Society of America, the Tom and Rose Bedwell Earth Physics Award, Pioneer Natural Resources, and the Friday Lunch Clubbe. Funding for V.C. Smith was provided by Natural Environment Research Council (UK) grant no. NE/5003584/1. K. Iacovino was supported by the NASA Jacobs JETS contract #NNJ13HA01C. G. Giordano acknowledges the grant to the Department of Science, Roma Tre University (MIUR–Italy Dipartimenti di Eccellenza, ARTICOLO 1, COMMI314–337 LEGGE 232/2016). We are thankful to Agnese Barbero and Francesco D'Assisi Tramparulo for their assistance in the field. We thank K. Wallace, C. Wilson, and three anonymous reviewers for their valuable comments on earlier versions of this manuscript.

REFERENCES CITED

Anikovich, M.V., Sinitsyn, A.A., Hoffecker, J.F., Holliday, V.T., Popov, V.V., Lisitsyn, S.N., Forman, S.L., Levkovskaya, G.M., Pospelova, G.A., Kuz'mina, I.E., Burova, N.D., Goldberg, P., Macphail, R.I., Giaccio, B., and Praslov, N.D., 2007, Early Upper Paleolithic in eastern Europe and implications for the dispersal of modern humans: Science, v. 315, p. 223–226, https://doi.org/10.1126/science.1133376.

Arienzo, I., Civetta, L., Heumann, A., Wörner, G., and Orsi, G., 2009, Isotopic evidence for open system processes within the Campanian Ignimbrite (Campi Flegrei-Italy) magma chamber: Bulletin of Volcanology, v. 71, p. 285–300, https://doi.org/10.1007/s00445-008-0223-0.

Arienzo, I., Heumann, A., Wörner, G., Civetta, L., and Orsi, G., 2011, Processes and timescales of magma evolution prior to the Campanian Ignimbrite eruption (Campi Flegrei, Italy): Earth and Planetary Science Letters, v. 306, p. 217–228, https://doi.org/10.1016/j.epsl.2011.04.002.

Cappelletti, P., Cerri, G., Colella, A., De'Gennaro, M., Langella, A., Perrotta, A., and Scarpati, C., 2003, Post-eruptive processes in the Campanian Ignimbrite: Mineralogy and Petrology, v. 79, p. 79–97, https://doi.org/10.1007/s00710-003-0003-7.

Caron, B., Sulpizio, R., Zanchetta, G., Siani, G., and Santacroce, R., 2010, The late Holocene to Pleistocene tephrostratigraphic record of Lake Ohrid (Albania): Comptes Rendus Geoscience, v. 342, p. 453–466, https://doi.org/10.1016/j.crte.2010.03.007.

Civetta, L., Orsi, G., Pappalardo, L., Fisher, R.V., Heiken, G., and Ort, M., 1997, Geochemical zoning, mingling, eruptive dynamics and depositional processes—The Campanian Ignimbrite, Campi Flegrei caldera, Italy: Journal of Volcanology and Geothermal Research, v. 75, p. 183–219, https://doi.org/10.1016/S0377-0273(96)00027-3.

Costa, A., Folch, A., Macedonio, G., Giaccio, B., Isaia, R., and Smith, V.C., 2012, Quantifying volcanic ash dispersal and impact of the Campanian Ignimbrite super-eruption: Geophysical Research Letters, v. 39, https://doi.org/10.1029/2012GL051605.

Cullen, V.L., Smith, V.C., and Arz, H.W., 2014, The detailed tephrostratigraphy of a core from the south-east Black Sea spanning the last ~60 ka: Journal of Quaternary Science, v. 29, p. 675–690, https://doi.org/10.1002/jqs.2739.

Damaschke, M., Sulpizio, R., Zanchetta, G., Wagner, B., Böhm, A., Nowaczyk, N., Rethemeyer, J., and Hilgers, A., 2013, Tephrostratigraphic studies on a sediment core from Lake Prespa in the Balkans: Climate of the Past, v. 9, p. 267–287, https://doi.org/10.5194/cp-9-267-2013.

De Natale, G., Troise, C., Mark, D., Mormone, A., Piochi, M., Di Vito, M.A., Isaia, R., Carlino, S., Barra, D., and Somma, R., 2016, The Campi Flegrei Deep Drilling Project (CFDDP): New insight on caldera structure, evolution and hazard implications for the Naples area (Southern Italy): Geochemistry, Geophysics, Geosystems, v. 17, p. 4836–4847, https://doi.org/10.1002/2015GC006183.

DeVivo, B., Rolandi, G., Gans, P.B., Calvert, A., Bohrson, W.A., Spera, F.J., and Belkin, H.E., 2001, New constraints on the pyroclastic eruptive history of the Campanian volcanic plain (Italy): Mineralogy and Petrology, v. 73, p. 47–65, https://doi.org/10.1007/s007100170010.

Di Girolamo, P., Ghiara, M.R., Lirer, L., Munno, R., Rolandi, G., and Stanzione, D., 1984, Vulcanologia e Petrologia dei Campi Flegrei: Bollettino della Società Geologica Italiana, v. 103, p. 349–413.

Di Salvo, S., 2018, Unravelling plumbing system dynamics linked to explosive eruptions by geochemical and isotopic micro-analyses: The case study of Campanian Ignimbrite, Campi Flegrei, Italy: Università degli studi di Firenze, 287 p.

Di Salvo, S., Avanzinelli, R., Isaia, R., Zanetti, A., Druitt, T.H., and Francalanci, L., 2020, Crystal-mush reactivation by magma recharge: Evidence from the Campanian Ignimbrite activity, Campi Flegrei volcanic field, Italy: Lithos, v. 376–377, https://doi.org/10.1016/j.lithos.2020.105780.

Dioguardi, F., Mele, D., Dellino, P., and Dürig, T., 2017, The terminal velocity of volcanic particles with shape obtained from 3-D X-ray microtomography: Journal of Volcanology and Geothermal Research, v. 329, p. 41–53, https://doi.org/10.1016/j.jvolgeores.2016.11.013.

Douka, K., Higham, T., and Sinitsyn, A., 2010, The influence of pretreatment chemistry on the radiocarbon dating of Campanian Ignimbrite-aged charcoal from Kostenki 14 (Russia): Quaternary Research, v. 73, p. 583–587, https://doi.org/10.1016/j.yqres.2010.01.002.

Dunbar, N.W., and Kyle, P.R., 1992, Volatile contents of obsidian clasts in tephra from the Taupo Volcanic Zone, New Zealand: Implications to eruptive processes: Journal of Volcanology and Geothermal Research, v. 49, p. 127–145, https://doi.org/10.1016/0377-0273(92)90009-3.

Dürig, T., Bowman, M.H., White, J.D.L., Murch, A., Mele, D., Verolino, A., and Dellino, P., 2018, Particle Shape Analyzer PARTISAN—An open source tool for multi-standard two-dimensional particle morphometry analysis: Annals of Geophysics, v. 61, p. 1–19, https://doi.org/10.4401/ag-7865.

Fedele, L., Scarpati, C., Lanphere, M., Melluso, L., Morra, V., Perrotta, A., and Ricci, G., 2008, The Breccia Museo formation, Campi Flegrei, southern Italy: Geochronology, chemostratigraphy and relationship with the Campanian Ignimbrite eruption: Bulletin of Volcanology, v. 70, p. 1189–1219, https://doi.org/10.1007/s00445-008-0197-y.

Fedele, L., Scarpati, C., Sparice, D., Perrotta, A., and Laiena, F., 2016, A chemostratigraphic study of the Campanian Ignimbrite eruption (Campi Flegrei, Italy): Insights on magma chamber withdrawal and deposit accumulation as revealed by compositionally zoned stratigraphic and facies framework: Journal of Volcanology and Geothermal Research, v. 324, p. 105–117, https://doi.org/10.1016/j.jvolgeores.2016.05.019.

Fisher, R.V., Orsi, G., Ort, M., and Heiken, G., 1993, Mobility of a large-volume pyroclastic flow—Emplacement of the Campanian ignimbrite, Italy: Journal of Volcanology and Geothermal Research, v. 56, p. 205–220, https://doi.org/10.1016/0377-0273(93)90017-L.

Forni, F., Bachmann, O., Mollo, S., De Astis, G., Gelman, S.E., and Ellis, B.S., 2016, The origin of a zoned ignimbrite: Insights into the Campanian Ignimbrite magma chamber (Campi Flegrei, Italy): Earth and Planetary Science Letters, v. 449, p. 259–271, https://doi.org/10.1016/j.epsl.2016.06.003.

Fulignati, P., Marianelli, P., Proto, M., and Sbrana, A., 2004, Evidences for disruption of a crystallizing front in a magma chamber during caldera collapse: An example from the Breccia Museo unit (Campanian Ignimbrite eruption, Italy): Journal of Volcanology and Geothermal Research, v. 133, p. 141–155, https://doi.org/10.1016/S0377-0273(03)00395-0.

Gardner, J.E., Andrews, B.J., and Dennen, R., 2017a, Liftoff of the 18 May 1980 surge of Mount St. Helens (USA) and the deposits left behind: Bulletin of Volcanology, v. 79, https://doi.org/10.1007/s00445-016-1095-3.

Gardner, J.E., Llewellin, E.W., Watkins, J.M., and Befus, K.S., 2017b, Formation of obsidian pyroclasts by sintering of ash particles in the volcanic conduit: Earth and Planetary Science Letters, v. 459, p. 252–263, https://doi.org/10.1016/j.epsl.2016.11.037.

Gebauer, S.K., Schmitt, A.K., Pappalardo, L., Stockli, D.F., and Lovera, O.M., 2014, Crystallization and eruption ages of Breccia Museo (Campi Flegrei caldera, Italy) plutonic clasts and their relation to the Campanian Ignimbrite: Contributions to Mineralogy and Petrology, v. 167, 953, https://doi.org/10.1007/s00410-013-0953-7.

Giaccio, B., Isaia, R., Fedele, F.G., Di Canzio, E., Hoffecker, J., Ronchitelli, A., Sinitsyn, A.A., Anikovich, M., Lisitsyn, S.N., and Popov, V.V., 2008, The Campanian Ignimbrite and Codola tephra layers: Two temporal/stratigraphic markers for the Early Upper Palaeolithic in southern Italy and eastern Europe: Journal of Volcanology and Geothermal Research, v. 177, p. 208–226, https://doi.org/10.1016/j.jvolgeores.2007.10.007.

Giaccio, B., Hajdas, I., Isaia, R., Deino, A., and Nomade, S., 2017, High-precision ^{14}C and $^{40}Ar/^{39}Ar$ dating of the Campanian Ignimbrite (Y-5) reconciles the time-scales of climatic-cultural processes at 40 ka: Scientific Reports, v. 7, https://doi.org/10.1038/srep45940.

Giordano, G., and Cas, R.A.F., 2021, Classification of ignimbrites and their eruptions: Earth-Science Reviews, v. 220, https://doi.org/10.1016/j.earscirev.2021.103697.

Hildreth, W., and Mahood, G.A., 1986, Ring-fracture eruption of the Bishop Tuff: Geological Society of America Bulletin, v. 97, p. 396–403, https://doi.org/10.1130/0016-7606(1986)97<396:REOTBT>2.0.CO;2.

Isaia, R., Iannuzzi, E., Sbrana, A., Marianelli, P., Donadio, C., Conforti, A., and D'Argenio, B., 2018, Note illustrative della Carta Geologica d'Italia alla scala 1:50.000: Istituto Superiore per la Protezione e la Ricerca Ambientale, Servizio Geologico d'Italia, 250 p.

Klug, C., and Cashman, K.V., 1996, Permeability development in vesiculating magmas: Implications for fragmentation: Bulletin of Volcanology, v. 58, p. 87–100, https://doi.org/10.1007/s004450050128.

Langella, A., Bish, D.L., Cappelletti, P., Cerri, G., Colella, A., de Gennaro, R., Graziano, S.F., Perrotta, A., Scarpati, C., and de Gennaro, M., 2013, New insights into the mineralogical facies distribution of Campanian Ignimbrite, a relevant Italian industrial material: Applied Clay Science, v. 72, p. 55–73, https://doi.org/10.1016/j.clay.2013.01.008.

Lirer, L., Rolandi, G., and Rubin, M., 1991, ^{14}C age of the "Museum Breccia" (Campi Flegrei) and its relevance for the origin of the Campanian Ignimbrite: Journal of Volcanology and Geothermal Research, v. 48, p. 223–227, https://doi.org/10.1016/0377-0273(91)90044-Z.

Matthews, I.P., Trincardi, F., Lowe, J.J., Bourne, A.J., MacLeod, A., Abbott, P.M., Andersen, N., Asioli, A., Blockley, S.P.E., Lane, C.S., Oh, Y.A., Satow, C.S., Staff, R.A.S., and Wulf, R.A., 2015, Developing a robust tephrochronological framework for Late Quaternary marine records in the Southern Adriatic Sea: New data from core station SA03–11: Quaternary Science Reviews, v. 118, p. 84–104, https://doi.org/10.1016/j.quascirev.2014.10.009.

Mele, D., and Dioguardi, F., 2018, The grain size dependency of vesicular particle shapes strongly affects the drag of particles. First results from microtomography investigations of Campi Flegrei fallout deposits: Journal of Volcanology and Geothermal Research, v. 353, p. 18–24, https://doi.org/10.1016/j.jvolgeores.2018.01.023.

Melluso, L., Morra, V., Perrotta, A., Scarpati, C., and Adabbo, M., 1995, The eruption of the Breccia Museo (Campi Flegrei, Italy): Fractional crystallization processes in a shallow, zoned magma chamber and implications for the eruptive dynamics: Journal of Volcanology and Geothermal Research, v. 68, p. 325–339, https://doi.org/10.1016/0377-0273(95)00020-5.

Orsi, G., De Vita, S., and di Vito, M., 1996, The restless, resurgent Campi Flegrei nested caldera (Italy): Constraints on its evolution and configuration: Journal of Volcanology and Geothermal Research, v. 74, p. 179–214, https://doi.org/10.1016/S0377-0273(96)00063-7.

Ort, M., Giordano, G., Zanella, E., Isaia, R., Silleni, A., and Smith, V.C., 2018, Supercharging a pyroclastic density current with caldera hydrothermal fluids: Campanian Ignimbrite, Italy: Cities on Volcanoes Conference, Naples, Italy, Session 01.17.

Ort, M.H., Rosi, M., and Anderson, C.D., 1999, Correlation of deposits and vent locations of the proximal Campanian Ignimbrite deposits, Campi Flegrei, Italy, based on natural remanent magnetization and anisotropy of magnetic susceptibility characteristics: Journal of Volcanology and Geothermal Research, v. 91, p. 167–178, https://doi.org/10.1016/S0377-0273(99)00034-7.

Ort, M.H., Orsi, G., Pappalardo, L., and Fisher, R.V., 2003, Anisotropy of magnetic susceptibility studies of depositional processes in the Campanian Ignimbrite, Italy: Bulletin of Volcanology, v. 65, p. 55–72, https://doi.org/10.1007/s00445-002-0241-2.

Pabst, S., Wörner, G., Civetta, L., and Tesoro, R., 2008, Magma chamber evolution prior to the Campanian Ignimbrite and Neapolitan Yellow Tuff eruptions (Campi Flegrei, Italy): Bulletin of Volcanology, v. 70, p. 961–976, https://doi.org/10.1007/s00445-007-0180-z.

Pappalardo, L., Civetta, L., D'Antonio, M., Deino, A., Di Vito, M., Orsi, G., Carandente, A., DeVita, S., Isaia, R., and Piochi, M., 1999, Chemical and Sr-isotopical evolution of the Phlegraean magmatic system before the Campanian Ignimbrite and the Neapolitan Yellow Tuff eruptions: Journal of Volcanology and Geothermal Research, v. 91, p. 141–166, https://doi.org/10.1016/S0377-0273(99)00033-5.

Perrotta, A., and Scarpati, C., 1994, The dynamics of the Breccia Museo eruption (Campi Flegrei, Italy) and the significance of spatter clasts associated with lithic breccias: Journal of Volcanology and Geothermal Research, v. 59, p. 335–355, https://doi.org/10.1016/0377-0273(94)90086-8.

Perrotta, A., and Scarpati, C., 2003, Volume partition between the Plinian and co-ignimbrite air fall deposits of the Campanian Ignimbrite eruption: Mineralogy and Petrology, v. 79, p. 67–78, https://doi.org/10.1007/s00710-003-0002-8.

Perrotta, A., Scarpati, C., Luongo, G., and Morra, V., 2006, Chapter 5: The Campi Flegrei caldera boundary in the city of Naples, *in* DeVivo, B., ed., Developments in Volcanology, v. 9, p. 85–96, https://doi.org/10.1016/S1871-644X(06)80019-7.

Perrotta, A., Scarpati, C., Luongo, G., and Morra, V., 2010, Stratigraphy and volcanological evolution of the southwestern sector of Campi Flegrei and Procida Island, Italy, *in* Groppelli, G., and Viereck-Goette, L., eds., Volcanism in the Campania Plain Vesuvius, Campi Flegrei and Ignimbrites: Stratigraphy and Geology of Volcanic Areas: Geological Society of America Special Paper 464, p. 171–191, https://doi.org/10.1130/2010.2464(09).

Pittari, A., Cas, R.A.F., Wolff, J.A., Nichols, H.J., Larson, P.B., and Martí, J., 2008, The use of lithic clast distributions in pyroclastic deposits to understand pre- and syn-caldera collapse processes: A case study of the Abrigo Ignimbrite, Tenerife, Canary Islands, *in* Gottsmann, J., and Martí, J., eds., Caldera Volcanism: Analysis, Modelling and Response: Developments in Volcanology, v. 10, p. 97–142, https://doi.org/10.1016/S1871-644X(07)00003-4.

Polacci, M., Pioli, L., and Rosi, M., 2003, The Plinian phase of the Campanian Ignimbrite eruption (phlegrean fields, Italy): Evidence from density measurements and textural characterization of pumice: Bulletin of Volcanology, v. 65, p. 418–432, https://doi.org/10.1007/s00445-002-0268-4.

Pyle, D.M., Ricketts, G.D., Margari, V., van Andel, T.H., Sinitsyn, A.A., Praslov, N.D., and Lisitsyn, S., 2006, Wide dispersal and deposition of distal tephra during the Pleistocene "Campanian Ignimbrite/Y5" eruption, Italy: Quaternary Science Reviews, v. 25, p. 2713–2728, https://doi.org/10.1016/j.quascirev.2006.06.008.

Rosi, M., Vezzoli, L., Aleotti, P., and De Censi, M., 1996, Interaction between caldera collapse and eruptive dynamics during the Campanian Ignimbrite eruption, Phlegraean Fields, Italy: Bulletin of Volcanology, v. 57, p. 541–554, https://doi.org/10.1007/BF00304438.

Rosi, M., Vezzoli, L., Castelmenzano, A., and Grieco, G., 1999, Plinian pumice fall deposit of the Campanian Ignimbrite eruption (Phlegraean Fields, Italy): Journal of Volcanology and Geothermal Research, v. 91, p. 179–198, https://doi.org/10.1016/S0377-0273(99)00035-9.

Ruberti, D., Vigliotti, M., Rolandi, R., and Di Lascio, M., 2020, Effect of paleomorphology on facies distribution of the Campania Ignimbrite in the northern Campania plain, southern Italy, *in* De Vivo, B., Belkin, H.E., and Rolandi, G., eds., Vesuvius, Campi Flegrei, and Campanian Volcanism: Cambridge, UK, Elsevier Inc., p. 207–229, https://doi.org/10.1016/B978-0-12-816454-9.00009-2.

Saxby, J., Beckett, F., Cashman, K., Rust, A., and Tennant, E., 2018, The impact of particle shape on fall velocity: Implications for volcanic ash dispersion modelling: Journal of Volcanology and Geothermal Research, v. 362, p. 32–48, https://doi.org/10.1016/j.jvolgeores.2018.08.006.

Scarpati, C., and Perrotta, A., 2012, Erosional characteristics and behavior of large pyroclastic density currents: Geology, v. 40, p. 1035–1038, https://doi.org/10.1130/G33380.1.

Scarpati, C., and Perrotta, A., 2016, Stratigraphy and physical parameters of the Plinian phase of the Campanian Ignimbrite eruption: Geological Society of America Bulletin, v. 128, p. 1147–1159, https://doi.org/10.1130/B31331.1.

Scarpati, C., Sparice, D., and Perrotta, A., 2015a, Facies variation in the Campanian Ignimbrite: Rendiconti Online Societa Geologica Italiana, v. 33, p. 83–87, https://doi.org/10.3301/ROL.2015.20.

Scarpati, C., Sparice, D., and Perrotta, A., 2015b, The ground layer of the Campanian Ignimbrite: An example of deposition from a dilute pyroclastic density current: Bulletin of Volcanology, v. 77, 97, https://doi.org/10.1007/s00445-015-0985-0.
Scarpati, C., Sparice, D., and Perrotta, A., 2020, Dynamics of large pyroclastic currents inferred by the internal architecture of the Campanian Ignimbrite: Scientific Reports, v. 10, 22230, https://doi.org/10.1038/s41598-020-79164-7.
Signorelli, S., Vaggelli, G., Francalanci, L., and Rosi, M., 1999, Origin of magmas feeding the Plinian phase of the Campanian Ignimbrite eruption, Phlegrean Fields (Italy): Constraints based on matrix-glass and glass-inclusion compositions: Journal of Volcanology and Geothermal Research, v. 91, p. 199–220, https://doi.org/10.1016/S0377-0273(99)00036-0.
Silleni, A., 2019, Magnitude, transport and deposition of the 40-ka large-volume Campanian Ignimbrite: Roma Tre Universita Degli Studi, 167 p.
Silleni, A., Giordano, G., Isaia, R., and Ort, M.H., 2020, The magnitude of the 39.8 ka Campanian Ignimbrite eruption, Italy: Method, uncertainties and errors: Frontiers of Earth Science, v. 8, https://doi.org/10.3389/feart.2020.543399.
Smith, V.C., Isaia, R., Engwell, S.L., and Albert, P.G., 2016, Tephra dispersal during the Campanian Ignimbrite (Italy) eruption: Implications for ultra-distal ash transport during the large caldera-forming eruption: Bulletin of Volcanology, v. 78, 45, https://doi.org/10.1007/s00445-016-1037-0.
Sparice, D., 2015, Definizione delle litofacies e ricostruzione dell'architettura dell'Ignimbrite Campana: Universita degli Stdi di Napoli Federico II, 241 p.
Suzuki-Kamata, K., Kamata, H., and Bacon, C.R., 1993, Evolution of the caldera-forming eruption at Crater Lake, Oregon, indicated by component analysis of lithic fragments: Journal of Geophysical Research: Solid Earth, v. 98, p. 14,059–14,074, https://doi.org/10.1029/93JB00934.
Vanorio, T., and Kanitpanyacharoen, W., 2015, Rock physics of fibrous rocks akin to Roman concrete explains uplift at Campi Flegrei Caldera: Scientific Reports, v. 349, p. 617–622.
Vinkler, A.P., Cashman, K., Giordano, G., and Groppelli, G., 2012, Evolution of the mafic Villa Senni caldera-forming eruption at Colli Albani volcano, Italy, indicated by textural analysis of juvenile fragments: Journal of Volcanology and Geothermal Research, v. 235–236, p. 37–54, https://doi.org/10.1016/j.jvolgeores.2012.03.006.
Vitale, S., and Ciarcia, S., 2018, Tectono-stratigraphic setting of the Campania region (southern Italy): Journal of Maps, v. 14, p. 9–21, https://doi.org/10.1080/17445647.2018.1424655.
Vitale, S., and Isaia, R., 2014, Fractures and faults in volcanic rocks (Campi Flegrei, southern Italy): Insight into volcano-tectonic processes: International Journal of Earth Sciences, v. 103, p. 801–819, https://doi.org/10.1007/s00531-013-0979-0.
Vogel, H., Zanchetta, G., Sulpizio, R., Wagner, B., and Nowaczyk, N., 2009, A tephrostratigraphic record for the last glacial–interglacial cycle from Lake Ohrid, Albania and Macedonia: Journal of Quaternary Science, v. 22, p. 311–320, https://10.1002/jqs.1311.
Wagner, B., Sulpizio, R., Zanchetta, G., Wulf, S., Wessels, M., Daut, G., and Nowaczyk, N., 2008, The last 40 ka tephrostratigraphic record of Lake Ohrid, Albania and Macedonia: A very distal archive for ash dispersal from Italian volcanoes: Journal of Volcanology and Geothermal Research, v. 177, p. 71–80, https://doi.org/10.1016/j.jvolgeores.2007.08.018.
Wilson, C.J.N.N., and Walker, G.P.L.L., 1982, Ignimbrite depositional facies: The anatomy of a pyroclastic flow: Journal of the Geological Society, v. 139, p. 581–592, https://doi.org/10.1144/gsjgs.139.5.0581.
Woods, A.W., and Wohletz, K., 1991, Dimensions and dynamics of co-ignimbrite eruption columns: Nature, v. 350, p. 225–227, https://doi.org/10.1038/350225a0.